Negative microfilm 62-3268
received from university

TREADO, Paul Albert, 1936-
NEUTRON-CAPTURE GAMMA RAYS OF BROMINE, COPPER, IRIDIUM, NICKEL, AND TUNGSTEN.

University of Michigan, Ph.D., 1962
Physics, nuclear

University Microfilms, Inc., Ann Arbor, Michigan

NEUTRON-CAPTURE GAMMA RAYS OF BROMINE, COPPER, IRIDIUM, NICKEL, AND TUNGSTEN

by
Paul Albert Treado

A dissertation submitted in partial fulfillment
of the requirements for the degree of
Doctor of Philosophy in the
University of Michigan
1961

Doctoral Committee:

Assistant Professor Paul R. Chagnon
Professor Charles L. Dolph
Professor John S. King
Associate Professor Noah Sherman
Professor Marcellus L. Wiedenbeck

ACKNOWLEDGEMENTS

I wish to thank the members of my committee for their interest and guidance. I am particularly indebted to Dr. Paul R. Chagnon for suggesting my research, and for contributing many ideas and continued encouragement throughout. I must also thank Mr. R. M. Woods Jr. and Dr. M. L. Wiedenbeck for many enlightening discussions, Mr. A. B. Miller for his help in installing much of the apparatus, and the Ford Nuclear Reactor Staff for their cooperation in the use of their facilities.

Further, I want to thank my wife Jean and my son Christopher for their patience and fine cooperation, as well as my parents and my wife's parents for their faithful support.

Lastly, I wish to express my sincere thanks to the Atomic Energy Commission for the financial support granted my research under contract AT(11-1)-724 and the National Science Foundation for the three fellowships granted me during this research.

TABLE OF CONTENTS

		Page
ACKNOWLEDGMENTS		ii
LIST OF TABLES		iv
LIST OF FIGURES		vi
CHAPTER I	INTRODUCTION	1
	A. Review of Previous Work	1
	B. The Present Experiment	8
	C. Results	10
CHAPTER II	NEUTRON CAPTURE GAMMA RAYS	12
	A. Neutron Interactions	12
	B. Radiative Capture	17
	C. Statistical Properties	19
	D. General Properties	23
CHAPTER III	APPARATUS	27
	A. Beam Collimation	27
	B. Detection Equipment	31
CHAPTER IV	PROCEDURE	39
	A. Spectrum Accumulation and Analysis	39
	B. Background Corrections	43
CHAPTER V	RESULTS	48
	A. Bromine Isotopes	48
	B. Natural Copper	55
	C. Natural Iridium	61
	D. Nickel Isotopes	67
	E. Tungsten Isotopes	78
APPENDIX		89
BIBLIOGRAPHY		90

LIST OF TABLES

Table		Page
I	Early Experimental Measurements of Neutron-Capture Gamma Rays	3
II	Recent Experimental Measurements of Neutron-Capture Gamma Rays	5
III	Background parameters	44
IV	Isotopic constitution of the bromine samples	48
V	Energies in Mev and intensities in photons per 100 captures in the individual isotope of the neutron-capture gamma rays from separated bromine isotopes	49
VI	Gamma ray energies and intensities of natural copper	58
VII	Neutron binding energies of copper	59
VIII	Comparison of capture gamma-ray energies (E_γ) with excitation energies (E_x) from (d,p) reactions in Cu^{64} and Cu^{66}	59
IX	Gamma ray energies and intensities of natural iridium	64
X	Isotopic constitution of the nickel samples	67
XI	Energies of neutron-capture gamma rays in natural nickel	68
XII	Energies in Mev and intensities in photons per 100 captures in the individual isotope of the neutron-capture gamma rays from separated nickel isotopes	74
XIII	Comparison of capture gamma-ray energies (E_γ) with excitation energies (E_x) from (d,p) reactions in Ni^{58} and Ni^{60}	76
XIV	Cross sections, masses and isotopic constitution of the tungsten samples	85

LIST OF TABLES (CONT'D)

Table		Page
XV	Energies in Mev and intensities in photons per 100 captures in the individual isotope of the neutron-capture gamma rays from separated tungsten isotopes	85
XVI	Neutron binding energies of tungsten	87

LIST OF FIGURES

Figure		Page
1	$\nu(E)$ for $\rho = \rho_0 e^{E/\tau}$	22
2	$\nu(E)$ for $\rho = \rho_0 e^{\sqrt{\alpha E}}$	22
3	Attenuation of gamma rays and neutrons by lead and bismuth beam-port inserts	28
4	Beam shielding and collimation arrangement in the beam-port of the reactor	29
5	Geometry of the sample, and external shielding	30
6	Scintillation crystal geometry in the three-crystal spectrometer	32
7	Block diagram of the 3-crystal spectrometer and electronics	33
8	Experimental geometry of the 3-crystal spectrometer	34
9	Gain change of the 3-crystal spectrometer	35
10	Efficiency of the 3-crystal spectrometer	36
11	(a) Singles spectrum of a Na^{24} source (b) Spectrum of the same source taken with the 3-crystal spectrometer	37
12	Chlorine 3-crystal neutron-capture gamma-ray spectrum	41
13	Chlorine single-crystal neutron-capture gamma-ray spectrum	41
14	The three components of the Nickel 62 background	46
15	Nickel 62 3-crystal background spectrum	47
16	3-crystal neutron-capture gamma-ray spectra of (a) Natural Bromine, (b) Bromine 80 and (c) Bromine 82	50

LIST OF FIGURES (CONT'D)

Figure		Page
17	Single-crystal neutron-capture gamma-ray spectra of (a) Natural Bromine, (b) Bromine 80 and (c) Bromine 82	51
18	Total-coincidence spectra of (a) Bromine 80 and (b) Bromine 82	52
19	Natural Copper 3-crystal neutron-capture gamma-ray spectrum	56
20	Natural Copper single-crystal neutron-capture gamma-ray spectrum	56
21	Iridium 3-crystal neutron-capture gamma-ray spectrum	62
22	Iridium single-crystal neutron-capture gamma-ray spectrum	63
23	3-crystal neutron-capture gamma-ray spectra of (a) Natural Nickel and (b) Nickel 59	69
	(c) Nickel 61 and (d) Nickel 63	70
24	Single-crystal neutron-capture gamma-ray spectra of (a) Natural Nickel and (b) Nickel 59	71
	(c) Nickel 61 and (d) Nickel 63	72
25	Total-coincidence spectra of (a) Nickel 59 and (b) Nickel 61	73
26	3-crystal neutron-capture gamma-ray spectra of (a) Natural Tungsten and (b) Tungsten 183	79
	(c) Tungsten 185 and (d) Tungsten 187	80
27	Single-crystal neutron-capture gamma-ray spectra of (a) Natural Tungsten and (b) Tungsten 183	81
	(c) Tungsten 185 and (d) Tungsten 187	82
28	Total-coincidence spectra of (a) Tungsten 183 and (b) Tungsten 185	83
	(c) Tungsten 187	84

CHAPTER I

INTRODUCTION

A. A Review of Previous Experiments

Thermal neutrons are absorbed or elastically scattered by nuclei. When a nucleus of mass M_A absorbs a thermal neutron, a highly excited nucleus of mass M_{A+1} is formed. In a few cases, of which lithium, nitrogen, and uranium are good examples, the product nucleus disintegrates by particle emission or by fission. For most product nuclei the emission of a charged particle is not energetically possible, or is greatly retarded by the coulomb barrier, and fission is not possible. Thus, the mode of decay is the emission of gamma radiation.

When a thermal neutron is absorbed by a nucleus, the event is referred to as neutron capture and its energy balance can be written as:

$$(M_A + M_n)c^2 + E_n = M_{A+1}c^2 + E$$

In this expression M_n is the mass of the neutron, while E_n and E are the incident-neutron and reaction energies, respectively. E_n for thermal neutrons is approximately 0.025 ev and is negligible when compared with E which is about 8 Mev. Thus $E-E_n$, the Q value of the reaction, is the binding energy of the last neutron in the nucleus $A+1$. It is the sum of the transition energies for the t transitions which comprise a particular cascade from the capture state to the

ground state of the $(A+1)^{th}$ nucleus. Q can be expressed by:

$$Q = \sum_t \left[E_{tr} + \frac{E_{tr}^2}{2 M_{A+1} C^2} \right]$$

where the second term in the sum is the nuclear recoil energy. For high energy gamma rays and light nuclei, the nuclear recoil term can be a few kev, but in most instances it can be neglected. The energy Q varies from 2.23 Mev to approximately 11 Mev for various nuclei and is released by gamma rays in direct and cascade transitions to the ground state. Most nuclei ($A \gtrsim 12$) have a large number of energy levels which allow many possible transitions, and consequently their gamma-ray spectra are complex.

Many persons, using almost as many methods, have investigated the complex structure of neutron-capture gamma-ray spectra. The first experimenters used radioactive Ra-Be and accelerator $D^2(d,n)He^3$ neutron sources. In more recent work reactors have been used as neutron sources. The detection methods of the neutron-capture investigations have been the same as those used in nuclear spectroscopy of radioactive nuclei.

The earliest investigators and the methods they employed are listed in Table I. Lea[1], using a Ra-Be neutron source with argon- and hydrogen-filled geiger counters and, believing that gamma rays produce a more intense ionization current in argon than in hydrogen, thought he found the capture gamma ray of hydrogen. Soon after, Amaldi et al.[2] completed an intense study of the neutron-capture phenomena and found

that neutrons slowed down by passage through a hydrogenous material were more readily captured than those coming directly from a Ra-Be source. Using paraffin as a moderator and geiger counters as detectors, they observed gamma radiation from many of the thirty elements they investigated. In ensuing experiments Fleischmann[3], Rasetti[4], Kikuchi et al.[5,6] and Griffiths and Szilard[7] attempted to determine the energies of the gamma rays found by Amaldi et al. During this time Aoki[8] and Fleischmann[9] made notable attempts to measure the relative intensities of the known capture gamma rays using Ra-Be and Po-Be sources of neutrons, various hydrogenous materials as moderators and geiger counters with aluminum absorbers.

TABLE I

Early Experimental Measurements of Neutron-Capture Gamma Rays

Investigators	Neutron Source	Detection Method	Date
Lea	Ra-Be	Hydrogen and Argon Geiger Counters	1934
Amaldi et al.	Ra-Be	Geiger Counters	1934
Fleischmann	Ra-Be	Geiger Counters	1935-1936
Rasetti	Ra-Be	Geiger Counters	1935
Kikuchi et al.	$D^2(d,n)He^3$	Geiger Counters	1936-1937
Griffiths and Szilard	Ra-Be	Geiger Counters	1937
Aoki	$D^2(d,n)He^3$	Geiger Counters with Absorbers	1937
Fleischmann	Ra-Be	Geiger Counters with Absorbers	1938

The results of these first experiments were meager because the neutron sources and the corresponding capture radiations were weak. The detectors could give little more than an estimate of the energy and intensity of the most energetic gamma ray emitted by each sample. Experimenters could not determine the shape of the gamma-ray spectra nor the energies of the more intense gamma rays. It became apparent that further study of the complex spectra would be feasible only with very sensitive detectors or very high neutron fluxes. Sensitive detectors would allow the use of weak sources, and high neutron fluxes would allow the use of inefficient, but precise, magnetic spectrometers. The advent of scintillation crystals (more sensitive detectors than geiger counters) and nuclear reactors (sources of high neutron fluxes) prompted many new and successful investigations of neutron-capture gamma rays.

These more recent investigations are tabulated in Table II. A few investigators employed scintillation crystals and weak Ra-Be neutron sources[10-13]. Their results were good, but still meager. Consequently, most experiments have been done using reactors as sources of neutrons.

TABLE II

Recent Experimental Measurements of Neutron-Capture Gamma Rays

Investigators	Neutron Source	Detection Method	Date
Muehlhouse	Reactor	Geiger Counters	1949
Kubitschek and Dancoff	Reactor	Geiger Counters with absorbers	1949
Moak and Dabbs	Reactor	Cloud Chamber	1949
Hammermesh	Reactor	D_2O-soaked Plates	1949-1951
Cameron et al.	Reactor	D_2O-soaked Plates	1950
Wilson	Reactor	Deuterium Ionization Chamber	1950
Meyerhoff et al.	Ra-Be	Scintillation crystal	1950
Pringle et al.	Ra-Be	Scintillation crystal	1950-1951
Hammermesh and Hummel	Reactor	Scintillation crystal	1951-1952
Reardon et al.	Ra-Be	Compton Scintillation Spectrometer	1953
Bartholomew et al.*	Reactor	Magnetic Pair Spectrometer	1953-1959
Motz	Reactor	Magnetic Lens Spectrometer	1952-1954
Hammermesh and Recksiedler	Reactor	Scintillation crystal	1954
Reier and Shamos	Reactor	Compton Scintillation Spectrometer	1955
Estulin et al.	Reactor	Scintillation crystal	1956-1960
Groshev et al.*	Reactor	Magnetic Compton Spectrometer	1956-1960

Hammermesh	Reactor	Bent-crystal Spectrometer	1957
Segel	Reactor	3-Crystal Pair Spectrometer	1958-1959
Carpenter *et al.*	Reactor	Bent-crystal Spectrometer	1958-1961
Draper *et al.*	Electron accelerator	Anti-coincidence Spectrometer	1959-1961
Patronis and Marshak	Reactor	Scintillation crystal	1959
Manning and Bartholomew	Reactor	Scintillation crystal	1959
Smither	Reactor	Scintillation crystal	1961
Bollinger and duToit	Reactor	Scintillation crystals	1961

* These groups have been the principal investigators. They have studied practically every element.

Reactors have been capable of generating high neutron fluxes, and usually the strong sources of capture radiation have been easily isolated from the reactors' radiation. Two methods of isolation have been used: (a) A collimated neutron beam is allowed to pass through a hole in the reactor shielding and to impinge upon a sample. Then a spectrometer is placed close to the sample and out of the way of the reactor beam. (b) The sample is placed in a high neutron flux close to the reactor and the capture radiation is viewed through a hole in the reactor shielding. The gamma rays of the reactor itself have been greatly reduced by placing bismuth inserts between the samples and the

reactor. In method (a) the bismuth block, which emits a negligible amount of capture radiation, acts as a source of thermal neutrons relatively free from gamma radiation and in (b) it screens the spectrometer from direct reactor gamma rays.

The neutron beam method, (a), has been used in conjunction with various detection schemes in many experiments. Geiger counters have been used to measure the average number of gamma rays emitted per neutron capture, the neutron-capture gamma-ray multiplicity [14, 15], while the photodisintegration of the deuteron has been used to measure capture gamma ray energies[16-19]. The externally-produced low-energy capture gamma rays have been investigated both with single-crystal scintillation spectrometers[20-23] and with bent-crystal diffraction spectrometers[24-26]. High energy and coincident gamma rays have been measured with multi-crystal scintillation spectrometers[27-29]. The polarization of capture gamma rays has also been investigated, using the external neutron beam method[30].

Using the external gamma-ray beam method, (b), and magnetic spectrometers, one Canadian and one Russian group have investigated the capture radiation of nearly all elements[31,32]. These groups have been the principal investigators of neutron-capture gamma-ray energies and intensities. A magnetic lens spectrometer[33], a bent-crystal diffraction spectrometer[34,35], and a Compton scintillation spectrometer[36] have also been employed with external gamma-ray beams.

Draper et al.[37] have devised a unique and very successful

method of investigation. Using an electron accelerator bremstrahlung beam to make neutrons by the $Be^9(\gamma,n)\,2He^4$ reaction, they employ an anti-coincidence scintillation spectrometer to detect the capture radiation.

At the present many of these investigations are still being pursued, while others employing more powerful reactors and more precise detection apparatus are being prepared. Compact, high-current deuteron accelerators are now commercially available and make good neutron generators. It can be assumed they will soon be employed in the ever-continuing search for more accurate data on neutron-capture gamma-ray spectra.

B. The Present Experiment

The experiment to be described was conceived to obtain information about the structure of nuclei occurring as the products in neutron-capture reactions. The original intent was to do coincidence measurements and, eventually, to measure angular correlations whenever feasible. These aims could not be realized because the available reactor and detection equipment were not well suited for such a study. However, by using a well-collimated external neutron beam, a three-crystal scintillation pair spectrometer and a single-crystal scintillation spectrometer, the neutron-capture gamma-ray spectra of small samples of material could be measured. With the two spectrometers in coincidence, it was possible also to

measure the total-coincidence spectra of some samples. A total-coincidence spectrum was obtained by putting one spectrometer in coincidence with all the gamma rays entering the other spectrometer.

Thus, samples of natural Bromine, Copper, Iridium, Nickel, and Tungsten, and separated isotope samples of Br^{79}, Br^{81}, Ni^{58}, Ni^{60}, Ni^{62}, W^{182}, W^{184}, and W^{186} were placed in a neutron beam and their spectra obtained. The separated isotopes were procured from the Atomic Energy Commission through the Isotope Loan Plan. The neutron beam was extracted from the Ford Nuclear Reactor at the University of Michigan. This reactor is similar to the ORNL Bulk Shielding Reactor. The three-crystal spectrometer was similar to those proposed by Johansson[38] and Hofstadter and McIntyre[39].

In the process of doing the experiment, five principal problems were solved. They were:

a. The extraction and measurement of a suitable neutron beam.

b. The construction of a three-crystal scintillation pair spectrometer for the detection of high-energy gamma rays.

c. The reduction of the inherent electronic instability of the detection equipment to an acceptable level.

d. The determination of the spectrometer efficiency and its mono-energetic line shape.

e. The determination of the background radiations accompanying any spectrum.

C. Results

There were two types of results obtained in this research: those from the neutron-capture gamma-ray spectra and those from the supplementary experiments. From the gamma-ray spectra of the three-crystal and single-crystal spectrometers, the energies and intensities of the gamma rays were determined and the neutron binding energies of the product nuclei were inferred. Most gamma rays observed from a natural sample were assigned to specific isotopes whenever samples of separated isotopes were investigated. Total-coincidence spectra generally confirmed the inferred neutron binding energies. The general shape of the spectrometer spectrawas in qualitative agreement with that predicted from a statistical model of the nucleus. Two observed spectral properties agreed with the nuclear shell model: (a) some nuclei had intense high energy lines; (b) there was a correlation between the intensities of these lines and those of the proton groups leading to the same final state in the corresponding (d,p) reaction.

To arrive at these results, supplementary measurements were necessary. There exists an inherent electronic instability in any scintillation detection system immersed in a strong neutron and gamma-ray radiation field. This instability was investigated and was minimized by minimizing, within the limits of the experiment, the radiation striking the phototubes and crystals and the ratio of the fast to total neutrons in the vicinity of the detection apparatus.

Also, the ratio of the neutron flux to the gamma-ray flux striking the targets was measured and optimized. Lastly, the efficiency and resolution of the three-crystal spectrometer, the resolution of the single-crystal spectrometer and the background radiations for any sample were determined.

CHAPTER II

NEUTRON CAPTURE GAMMA RAYS

A. Neutron Reactions

Neutron bombardment of a nucleus can produce various reactions: elastic and inelastic scattering, capture followed by charged particle or gamma ray emission, and fission. The cross sections for these reactions depend on the incoming-neutron energy, the nucleus bombarded, and the products of the reaction. The general shape and resonance structure of these cross sections have been derived.

When both the initial and final states of the system consist of a pair of unbound particles, the transition is to one of a continuous distribution of states. Quantum mechanics gives the transition probability, the number of transitions per unit time, to be[40]:

$$P_1 = \frac{2\pi}{\hbar}|\mathcal{H}|^2\frac{dn}{dE}$$

for a direct interaction, where $\mathcal{H}$ is the matrix element of the perturbation causing the transition and dn/dE is the energy density of the final states. The density of states available to a free particle "b", which appears in the reaction (A + n → B + b), confined to a box of unit volume and having momentum between p and p + dp with spin I_b, is:

$$\frac{dn}{dE} = \frac{4\pi p_b^2}{(2\pi\hbar)^3 v_b}(2I_b+1)(2I_B+1)$$

where I_B is the spin of the residual nucleus. Then the cross section for the reaction can be written[41]:

$$\sigma_{m,b} = \frac{1}{\pi\hbar^4}|\mathcal{H}|^2 \frac{p_b^2}{V_m V_b}(2I_b+1)(2I_B+1)$$

$\mathcal{H}$ has the form $\int \psi_f^* U \psi_i \, dV$, where U is the interaction energy and the ψ 's are normalized in a box of unit volume.

To show the meaning of $\mathcal{H}$, it can be represented by

$$|\mathcal{H}| = \bar{U} \times \text{NUCLEAR VOLUME} \times |\overline{\psi_i \psi_f}|$$

where $|\overline{\psi_i \psi_f}|$ is a suitable average of the product of the wave functions over the volume of the nucleus, and $\bar{U}$ is some average interaction energy. $\mathcal{H}$ depends on the charge of the participating particles. If "b" is positively charged, its wave function will be reduced in amplitude outside of the nucleus by a factor, $\exp(-G_b/2)$, representing the Coulomb barrier. A neutron sees no Coulomb barrier and consequently its wave function is not reduced inside the nucleus.

In most cases, the matrix elements as a function of energy have irregularities called resonances. The formation of an intermediate system, a compound nucleus, has been assumed to explain the resonance structure of some cross sections[42]. When the lifetime of the compound nucleus is neglected, the transition probability for the reaction $(A + n \rightarrow C \rightarrow B + b)$ has been shown to be[40]

$$P_2 = \frac{2\pi}{\hbar}\left|\frac{\mathcal{H}_{cA}\mathcal{H}_{Bc}}{E_A - E_c}\right|^2 \frac{dm}{dE}$$

where $\mathcal{H}_{cA}$ has the form $\int \psi_c^* U \psi_A \, dV$ and $\mathcal{H}_{Bc}$ is similar, while E_A and E_C are the energies of the initial and compound-nucleus systems, respectively. Then the cross section is

$$\sigma_{m,b}^{r} = \frac{1}{\pi\hbar} \left| \frac{\mathcal{H}_{cA}\mathcal{H}_{Bc}}{E_A - E_c} \right|^2 \frac{p_b^2}{v_m v_b}$$

This expression for the cross section has a singularity as $E_A \longrightarrow E_C$. If, however, the lifetime of the compound nucleus is assumed long enough for the nucleus C to forget how it was formed, it has been shown that the expression for the cross section is[40]

$$\sigma_{m,b}^{r} = 4\pi \lambda\!\!\!^{-} \lambda\!\!\!^{-}_R \frac{\Gamma_b \Gamma_m^R}{\Gamma^2 + (\delta E)^2} g$$

which remains finite as $E_A \longrightarrow E_C$, at a resonance. In this expression

$$\lambda\!\!\!^{-} = \frac{\hbar}{mv}, \quad \lambda\!\!\!^{-}_R = \frac{\hbar}{mv_R}, \quad \Gamma_b = \frac{\hbar}{2\tau_b}, \quad \Gamma_m^R = \Gamma_m \frac{v_R}{v}, \quad \delta E = E_c - E_A$$

where M is the neutron's mass, v is the neutron's velocity, v_R is the neutron's resonance velocity and τ_b is the half-life of the state emitting "b". 'g' is a spin factor due to the multiplicity of angular momentum allowed in the resonance capture of thermal neutrons. In slow neutron reactions usually only the s-wave component of the neutron is involved and only compound nucleus states with $I_C = I_A \pm \frac{1}{2}$ are formed. Then 'g' is

$$g = \frac{1}{2}\left(1 \pm \frac{1}{2I_A + 1}\right)$$

where the + is used if $I_C = I_A + \frac{1}{2}$, and the - if $I_C = I_A - \frac{1}{2}$.

The general shape of these cross sections can now be plotted with a resonance peak superposed. In elastic scattering, (n,n), v_n equals v_b, so $p_b^2/v_n v_b = M_n^2$, which is a constant, and at non-resonant low energies $|\mathcal{H}|$ is approximately a constant; therefore the cross section is approximately a constant at low energies.

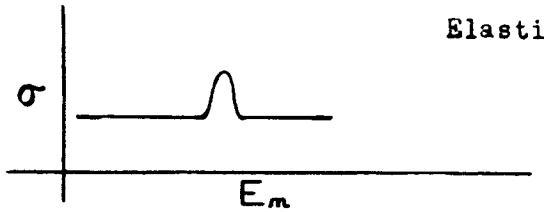

Elastic Scattering

Inelastic scattering processes are endothermic and near the threshold the cross section is proportional to (energy excess) $^{\frac{1}{2}}$.

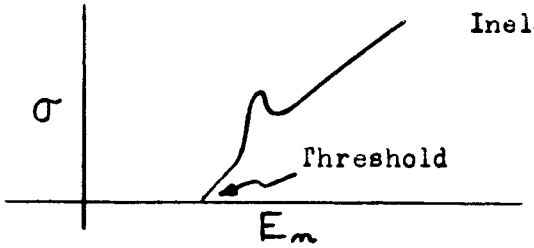

Inelastic Scattering

Neutron-capture processes can be exothermic or endothermic. When a thermal neutron is captured in an exothermic process, v_b is approximately constant and $|\mathcal{H}|$ is proportional to $\exp(-G_b)$. Because $\exp(-G_b)$ is constant, and $p_b^2/v_n v_b$ is proportional to $1/v_n$, the cross section is proportional to $1/v_n$. Hence:

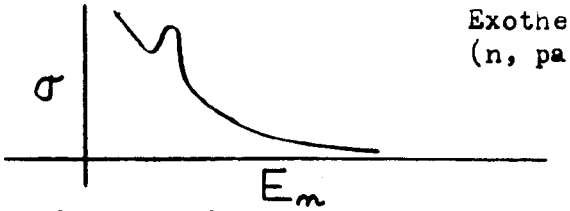

Exothermic Reactions
(n, particle),(n, γ)

The cross section for an endothermic reaction is similar to the inelastic scattering case, except that the factor $\exp(-G_b)$ for the

outgoing particle is dominant. The cross section is proportional to $(\text{energy excess})^{\frac{1}{2}} \exp(-G_b)$.

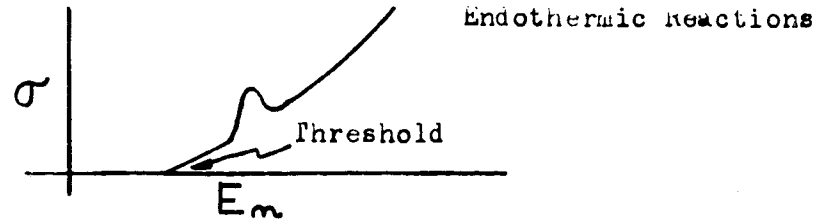

The fission phenomena can be best explained by a liquid drop model. The change in potential energy when the nuclear drop is deformed from a spherical shape can be estimated and if the energy decreases, the drop is stable. The spherical drop has been shown to be stable for $Z^2/A \lesssim 45$[43].

In this research thermal neutrons impinged upon various nuclei. The only reactions taking place were (n,n) and (n,γ) ones because:

(a) The incoming neutron energy was below the threshold energy for both inelastic scattering and endothermic reactions.

(b) None of the nuclei bombarded had a high enough A to allow fission.

(c) Charged particle emission was retarded by the high Coulomb barrier. (Only low Z elements, i.e., lithium and nitrogen, have appreciable (n, particle) cross sections.)

For the nuclei investigated the (n, γ) cross section was comparable with the (n,n) one because of resonances and the "1/v" law. Elastically scattered neutrons were present, however, and contributed to the background as will be shown in Chapter IV.

B. Radiative Capture

Two types of radiative capture mechanisms have been described in the literature[44,45,46]. In one the capture is direct and in the other a compound nucleus is formed. The cross sections for these processes have been determined by Lane and Lynn[44], using nuclear dispersion theory.

"Direct capture" implies that the nucleus is able to undergo a radiative transition before the incoming neutron shares its excitation energy with the target nucleons, i.e., before a compound nucleus is formed. An incident particle may move an appreciable distance through a target nucleus before a compound nucleus is formed. If, during the initial period of free motion in the mean nuclear potential, the particle radiates a photon and drops into a bound particle orbit, then it is captured directly. The formation of a compound nucleus leads to resonances in the radiative capture cross section and, for low-energy incoming particles, most capture reactions proceed through the formation and decay of a compound nucleus. However, direct capture may be comparable to compound nucleus formation, when capture occurs far from resonances in nuclei where the level spacings are large, and when radiative transitions can occur to levels which are relatively pure single particle states for the added neutron.

Starting from nuclear dispersion theory, the scattering matrix element and the capture cross section have been derived. They consist of three parts: a conventional resonance part, an anomalous resonance

part exhibiting selection rules, and a part accounting for single particle capture in the nuclear potential.

The conventional resonance part is due to compound nucleus formation. Lane and Lynn[44] have derived an expression for the contribution to the capture cross section from conventional resonance capture, i.e., the type qualitatively presented in Section A of this chapter. They did this by assuming the contribution was due only to levels of the compound nucleus near the incident energy. They also obtained expressions for the contribution to the cross section from the anomalous resonance and the direct capture mechanisms. The important feature of the latter mechanisms is that they tend to select final single-particle states and so give rise to intense lines in the photon spectrum. In fact, they showed that for s-wave capture, E1 transitions which involve final states having large admixtures of a single particle p-wave configuration should be strongly enhanced.

The general predictions of the direct capture formalism can give at least a qualitative explanation of the disagreement with statistical theory which is observed in (n, γ) spectra; namely, of the intense lines at the high energy end of the (n, γ) spectra.

This effect is outstanding in the spectra from nuclei with A approximately 50 and 190. For A near 50 it appears to be associated with a selection rule operating in accordance with anomalous resonance capture, while in the heavy isotope region there is evidence that it is a consequence of the direct capture mechanism.

The predictions of Lane and Lynn will be compared in Chapter V with the indications of the spectra measured in this research.

C. Statistical Properties

Experimental evidence indicates that capture gamma-ray spectra from heavier nuclei are all similar. Thus, because nuclei are many particle systems, it may be that the spectra are determined essentially by the nuclear level density and by the multipolarity of the gamma transitions, and are only slightly altered by the specific properties of the transition matrix elements. If this were true it would be possible to predict the shape of the (n, γ) spectra by first obtaining $\rho(E,Z,N)$, the nuclear energy level density, and then computing $\nu(E)$, the number of photons per neutron capture per unit energy interval, from $\rho(E,Z,N)$. The determination of $\nu(E)$ from $\rho(E,Z,N)$, which is made difficult by the multitude of paths available for a transition from the excited state to the ground state, has been done by Strutinskii et al.[47]. $\rho(E,Z,N)$ is slightly model-dependent and it was hoped that experimental evidence would favor one model's density. Nuclear level densities have been determined for various models. Three of these are presented below.

A. Free Particle Model: It was assumed that the nucleus consists of Z protons and N neutrons moving as free particles in a volume V, which is a simple function of the number of nucleons. This system is a degenerate Fermi-Dirac gas in volume V. ρ was found to be[48]:

$$\rho = \alpha_0 \frac{A^{3/4}}{E^{7/4}} e^{\beta_0 \sqrt{E}}$$

B. Independent Particle Model: The particles were assumed independent, but not free, in V. ρ was determined by van Lier and Uhlenbeck[4], using Sommerfeld's theorem, to be:

$$\rho = \frac{\alpha_1}{E^{5/2}} A^{1/2} e^{\beta_1 \sqrt{E}}$$

C. Liquid Drop Model: Assuming surface wave vibrations, a Planck distribution for the average energy of the ith vibration and Bose-Einstein statistics for the quasi-particle vibrations, ρ was found to be:

$$\rho = \gamma(E) A^{2/3} e^{\beta_2 E^{4/7}}$$

In these expressions the α_i and β_i are constants. It should be noted that ρ does not vary significantly from model to model. Thus, the experimentally measured spectra can give little information as to what is the best model to represent a particular nucleus.

To predict the total gamma spectrum the spectra of all cascades must be summed. Assuming the energy of the emitted quanta is small

compared with the nuclear excitation energy, the number of quanta in E to E + dE, $\nu(E)dE$, is

$$\nu(E)\,dE = dE\int_{E}^{u_0}\frac{\omega(u,E)\,du}{\overline{E}(u)}$$

and the total number of quanta emitted, $\overline{\nu}$, is

$$\overline{\nu} \equiv \int_0^{u_0}\nu(E)\,dE = \int_0^{u_0}\frac{du}{\overline{E}(u)}$$

where u_0 is the initial excitation energy, $\overline{E}(u) = \int_0^u \omega(u,E)\,E\,dE$ and $w(u,E)$ is the relative probability of emission of a gamma quantum of energy E by a nucleus located in a state of energy u. In accordance with statistical theory and in agreement with Blatt and Weisskopf[50], $w(u,E)$ is

$$\omega(u,E) = \frac{E^{2l+1}\,\rho(u-E)}{n(u)}$$

where l is the radiation multipolarity, $\rho(u-E)$ is the level density, and $n(u)$ is a normalizing factor:

$$n(u) = \int_0^u E^{2l+1}\rho(u-E)\,dE$$

Comparing this to experimental data one finds fair qualitative agreement, but one finds 3-4 quanta per capture and $\overline{E}$ is approximately 1.5-2.0 Mev, i.e., it is far from small compared with the nuclear excitation energy. Strutinskii showed that it is better to approximate

the gamma-ray spectrum on the basis of the kinetic equation which describes a gamma cascade process in nuclear decay. Then, assuming only dipole transitions and energy independence of the transition matrix elements, he obtained $\nu(E)$ in integral form, and evaluated it by means of a computer for level densities $\rho = \rho_0 e^{E/\tau}$ and $\rho = \rho_0 e^{\sqrt{\alpha E}}$ and for odd-odd and even-even nuclei[47]. The results are reproduced in Figures 1 and 2.

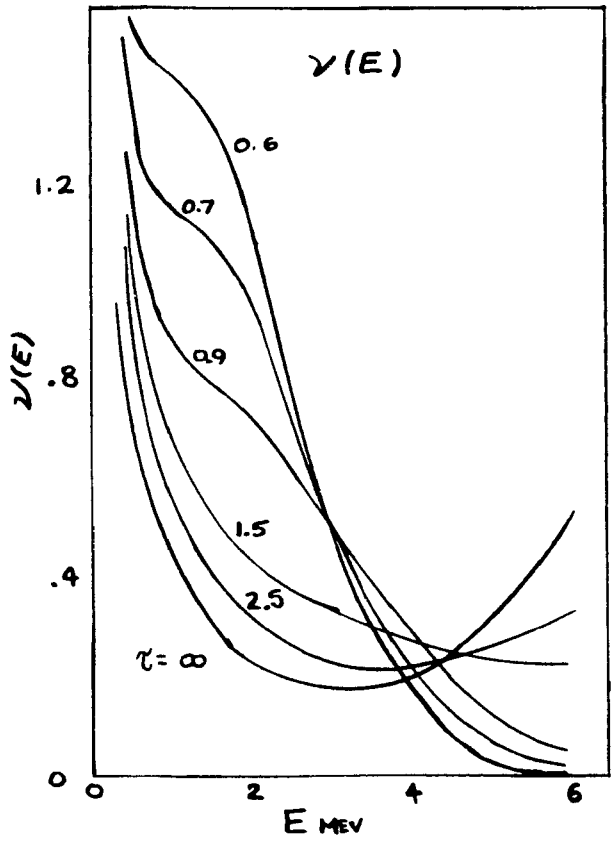

Figure 1. $\nu(E)$ for $\rho = \rho_0 e^{E/\tau}$

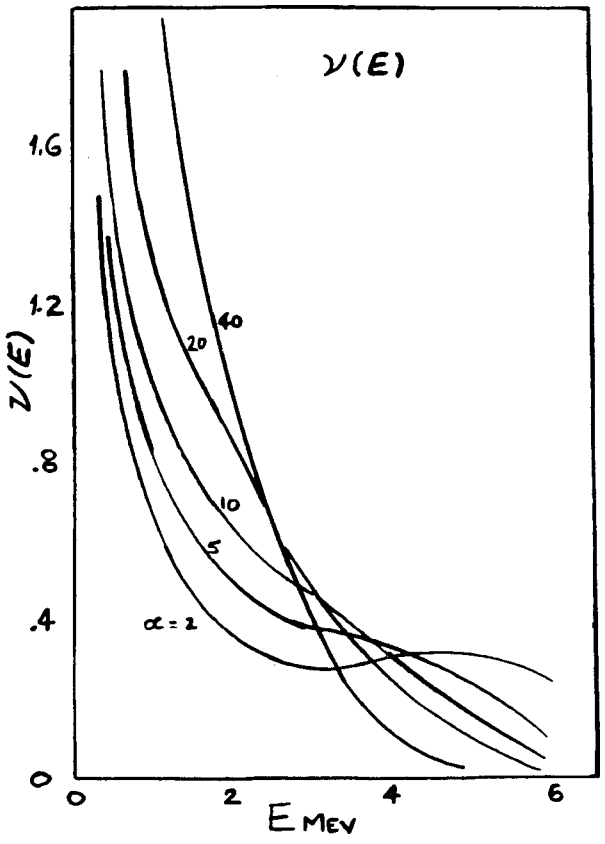

Figure 2. $\nu(E)$ for $\rho = \rho_0 e^{\sqrt{\alpha E}}$

An examination of the experimentally measured spectra reveals: for spherical odd-odd nuclei ($A \sim 110$), $\rho(E) = \rho_0 e^{\sqrt{\alpha E}}$ with

$\alpha = 15$ Mev^{-1} gives the best agreement, while for prolate odd-odd nuclei ($A \sim 175$), $\rho = \rho_0 e^{E/\tau}$ with $\tau = 0.8$ Mev fits best and for even-even nuclei either level density is acceptable.

From this and the approximations of the level density as a function of model, it seems that spherical odd-odd nuclei may be best represented by a shell model, and prolate odd-odd nuclei may be best represented by a collective model. With the present experimental techniques and the existing predictions of the general shape of the neutron-capture gamma-ray spectra, however, no clear indication of a variation of spectrum shape as a function of nuclear model can be observed.

D. General Properties

The shape of neutron-capture gamma-ray spectra and the information they provide depend directly on the manner in which the neutron is captured. Thermal neutron capture proceeds almost entirely by s-wave capture because of the centrifugal barrier for higher angular momentum. It has been shown that the ratio of s-wave to p-wave penetrabilities is:

$$\frac{P_s}{P_p} = 1 + \frac{1}{(KR)^2}$$

where R is the interaction radius and k is the neutron wave number[51]. This ratio is approximately 10^7 for thermal neutrons. For s-wave capture, both the target nucleus and the capture state have the same

parity and

$$J' = J_t \pm 1/2$$

where J' and J_t are the spins of the capture state and target nucleus, respectively.

In conventional resonance capture the details of the subsequent gamma-ray decay will be determined by the properties of the resonance leading to the compound nucleus. In non-resonant compound nucleus capture, both spin states will be present in the compound nucleus with their mixture depending on the shape and proximity of the two J' levels. As has been pointed out in Section B of this chapter, in non-resonant direct capture the transitions depend on the states of the product nucleus.

The information which can be obtained from neutron-capture gamma-ray spectra is limited by the incoming s-waves. This prohibits the determination of any useful spin information from (n, γ) angular distribution measurements and prohibits the studying of modes of decay from capture levels of either parity and many spin values.

The capture gamma-ray spectra have many properties which are of interest. The spectra of odd-odd product nuclei tend to be more complicated, particularly at high energies, than the spectra of the neighboring even-even or even-odd nuclei. It is thought that this is caused by differences in level density at the same excitation energy in the different types of nuclei. The level densities at low excitation

energies are less for even-nucleon type nuclei than for odd-odd nuclei because of the pairing energy which depresses the energy of the ground state configuration with respect to the lower excited levels, and must be supplied to the nucleus before single particle excitations can occur. Those parts of the spectra corresponding to transitions to levels above the pairing energy are similar for the three types of nuclei. Also, intense lines tend to concentrate at the high energy end of the low-A capture spectra, but in heavier nuclei the centroid of the more complex spectra moves to lower energies.

Some properties of the spectra seem to be related to the shell model of the nucleus. The spectra of light elements belonging to the same neutron shell have similar characteristics. Experimental intensities for light nuclei are in agreement with the ratio of E1:M1:E2 transitions which have been predicted[50,52]. Some spectra have very intense lines in the high-energy region. It is possible that the direct capture plays a role and in such cases the radiative transition may only involve a change in the neutron state while the target-nucleus core remains essentially undistrubed. Also there is an observed correlation between the intensities of some neutron-capture gamma rays and those of the proton groups leading to the same final state in the corresponding (d,p) reaction. It has been pointed out that the matrix elements for both reactions have a common part involving the parentage overlap of the initial and final states[53,54]. Lastly, the spectra of heavy elements have high-energy gamma rays

which can be associated with transitions of a single particle type leaving the core undisturbed.

Because the low-lying lines of the spectra are not precisely determined in most (n,γ) experiments, the collective model is seldom employed. Only in the spectra of medium A nuclei, where intense lines exist near 1 Mev, are the transitions assumed to be between members of neighboring rotational bands.

The discussions of this chapter will be employed in Chapter V in attempts to explain the spectra measured in this research.

CHAPTER III

APPARATUS

A. Beam Collimation and Shielding

A neutron beam, with a relatively small gamma-ray flux, was extracted from the Ford Nuclear Reactor through a beam port by means of a specially designed plug. The plug was designed by Dr. Paul R. Chagnon, and has been discussed previously[29,55].

The assembly proper of the Ford Nuclear Reactor is a cubic core, a meter on a side, immersed in a pool of demineralized water, which is surrounded by a two meter thick concrete shield. There exists several beam ports, which run from just outside the reactor core through the water and concrete to the reactor face. Preliminary measurements determined the flux at the reactor face from an open port to be approximately 5×10^8 nt/cm^2 sec, with a gamma-ray intensity of 100 R/hr.

It was necessary to reduce the gamma rays to a few hundred mR/hr, while making the neutron-to-gamma ray ratio as high as possible. The use of a Bragg scatterer to deflect the neutrons was considered, but a sufficiently high neutron intensity could not have been realized. Consequently, it was necessary to place a bismuth filter at the core end of the beam port. Bismuth has a high absorption cross section for gamma rays, while its neutron-capture cross section is only 32 mb. Bismuth's neutron-scattering cross section is appreciable ($\sigma = 9$ barns), so it had to be placed close to the core, and had to be limited in amount. Lead was also used, as it is similar to bismuth, but cheaper.

Figure 3 shows the effect of various thicknesses of filters on the neutron and gamma-ray intensities from an open beam port.

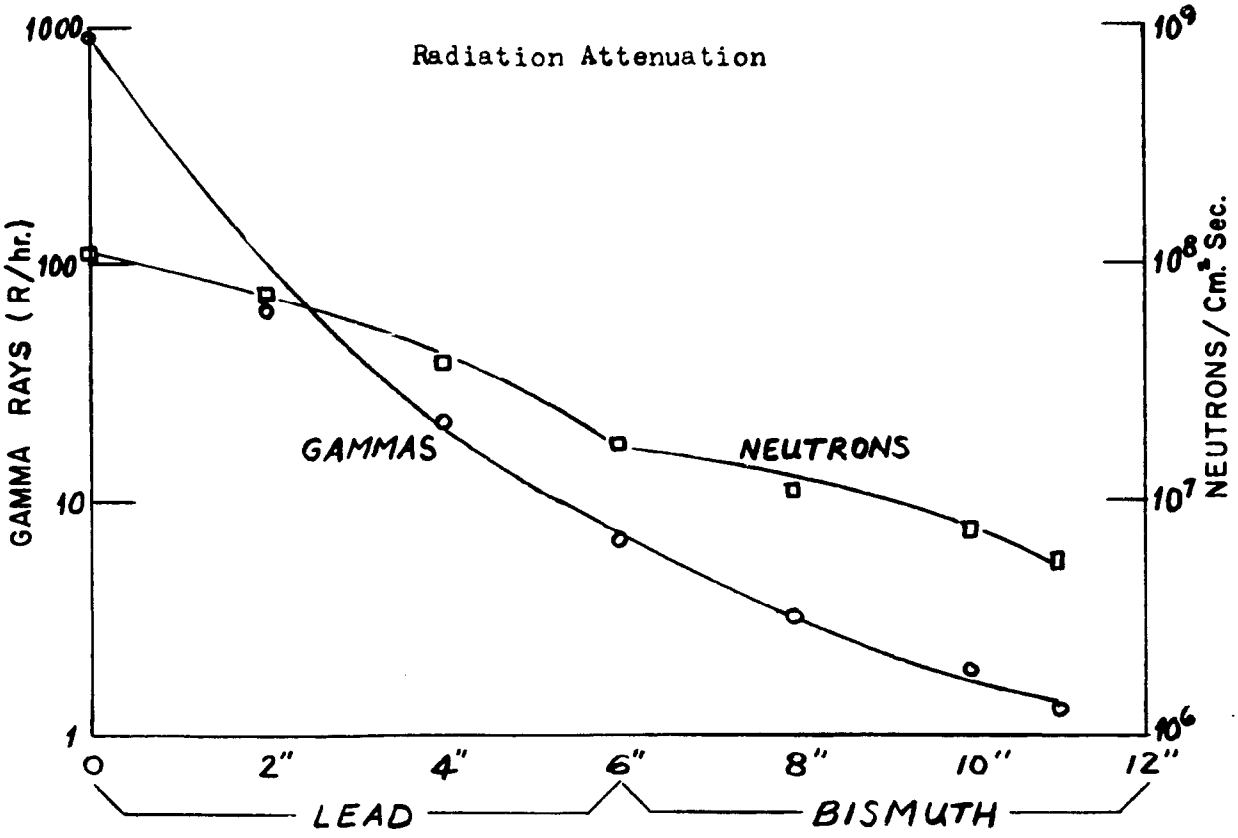

Figure 3. Attenuation of gamma rays and neutrons by lead and bismuth beam-port inserts.

As can be seen, addition of more than 8 in. of material did little to improve the neutron-to-gamma ratio. By proper shielding and collimation, the gamma-ray intensity was reduced by a factor of 10 and the neutron flux remained approximately 10^6nt/cm^2 sec.

Thus, the beam-port plug illustrated in Figure 4 was constructed and installed. The front 6 in. of filter was fixed on the end of the plug, and was lead; a 3 in. bismuth insert was also used.

Beam-Port Plug

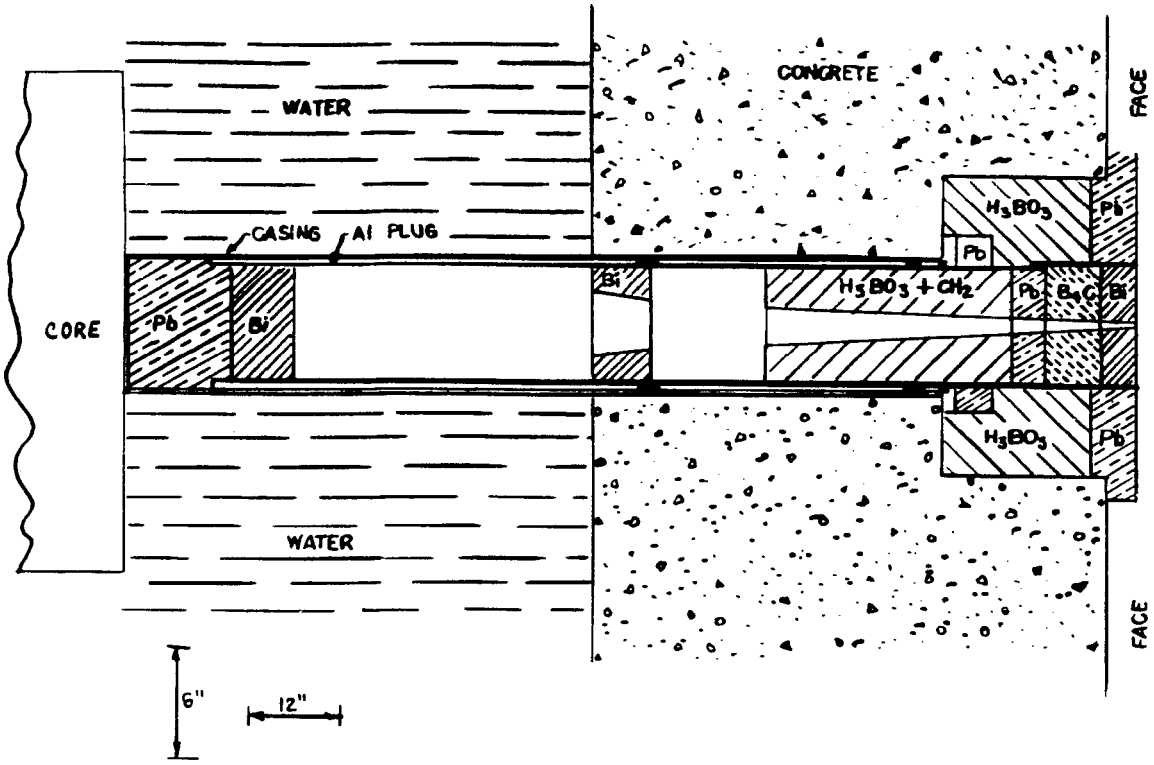

Figure 4. Beam shielding and collimation arrangement in the beam-port of the reactor.

Other inserts in the tube shielded against gamma rays, while the boric acid cylinder collimated the neutron beam. The collimator terminated in a 1/2 in. diameter hole at the reactor face. The plug had provisions for flooding the port with water to shut the beam off when required.

The intensities of the gamma-ray and neutron beams were measured with the reactor at 1 Megawatt. Using a cutie-pie ionization chamber, the gamma intensity was found to be approximately 250 mR/hr.

The thermal-neutron beam was determined by direct measurements of the 468 kev Ir^{192} radioactive gamma ray, and the 411 kev Au^{198} radioactive gamma ray. The rate of neutron capture was measured to be $(3.4 \pm 1.2) \times 10^5$ nt/cm^2 sec. This figure was in good agreement with the value inferred from the background measurements to be discussed in the next chapter.

External shielding to protect the personnel was required. It was constructed as shown in Figure 5 with a beam stopper and surrounding concrete blocks. The beam stopper was a steel tank, 4 ft. on a side, filled with boric acid and water.

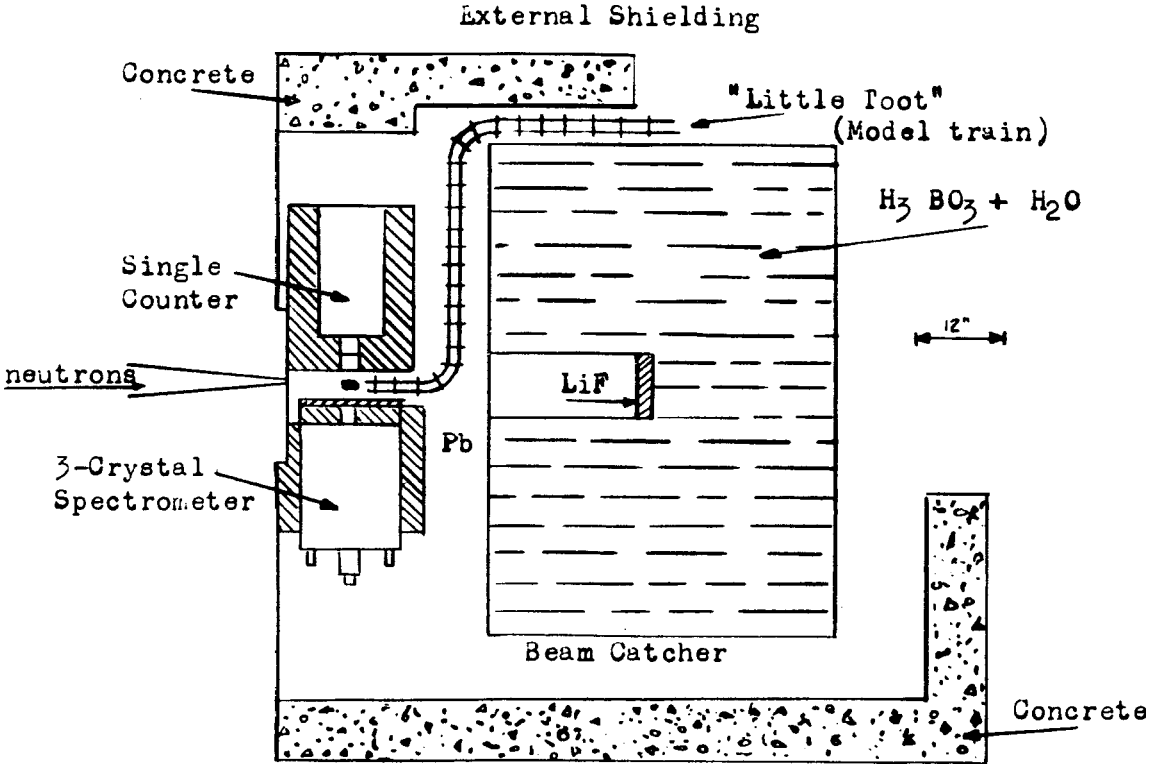

Figure 5. Geometry of the sample, counters, and external shielding.

The HO-gauge model electric train shown in the figure was used to change samples when the reactor was in operation.

B. Detection Equipment

The gamma-ray spectra observed in this experiment were detected by means of a single scintillation crystal, a three-crystal spectrometer, and the two in coincidence. The single crystal was used in the 0-2.0 Mev range and the three-crystal spectrometer in the 1.5-10.0 Mev range.

Johansson[38] and Hofstadter[39] proposed the use of a three-crystal scintillation spectrometer for the detection of high energy gamma rays. The idea was to select only one of the many possible interactions of a gamma ray with a crystal, namely, pair production followed by escape of both annihilation quanta. This would result in one peak in the pulse-height distribution for each line in the gamma-ray spectrum.

The spectrometer constructed for this research is shown in Figure 6. It had two sets of two scintillation counters (A and A', B and B') on each side of the primary detecting crystal. A and B were 1 3/4 in. by 2 in., and A' and B' were 2 in. by 2 in. NaI(Tl) crystals, while P was a 1 1/4 in. by 1 1/2 in. crystal. All were mounted on 6342A photomultipliers.

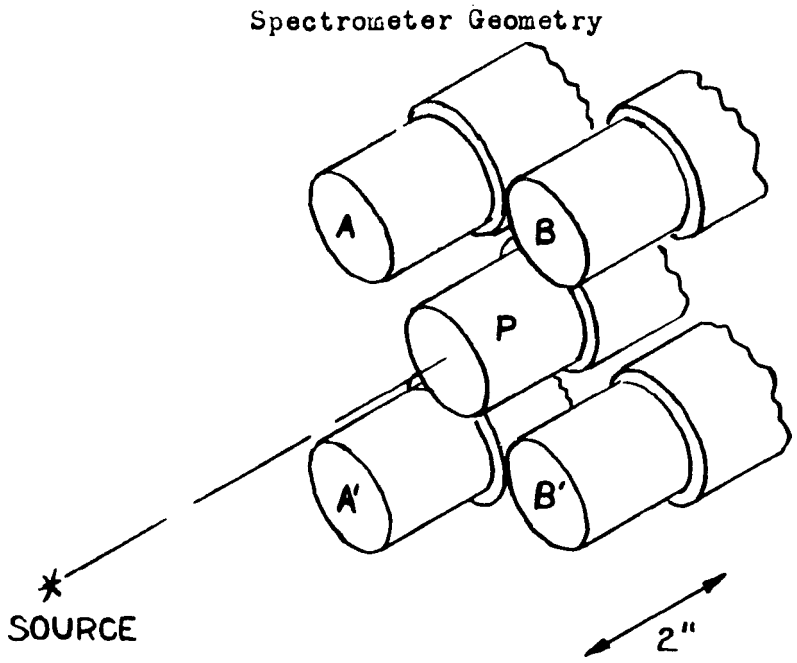

Figure 6. Scintillation crystal geometry in the three-crystal spectrometer.

A block diagram of the electronics used with the spectrometers is shown in Figure 7. For the three-crystal spectrometer; in order for a count to be recorded in the analyzer, a fast (10^{-8} sec) coincidence was required among the three sets of counters; in addition, the side counter pulses had to pass through single-channel discriminators set over the annihilation peak; these requirements having been met, the pulse from P passed through a linear gate and was recorded on the 256-channel analyzer. The single scintillation crystal was fed directly into the analyzer. The fast amplifiers and linear gates were designed by Dr. Paul Chagnon[56].

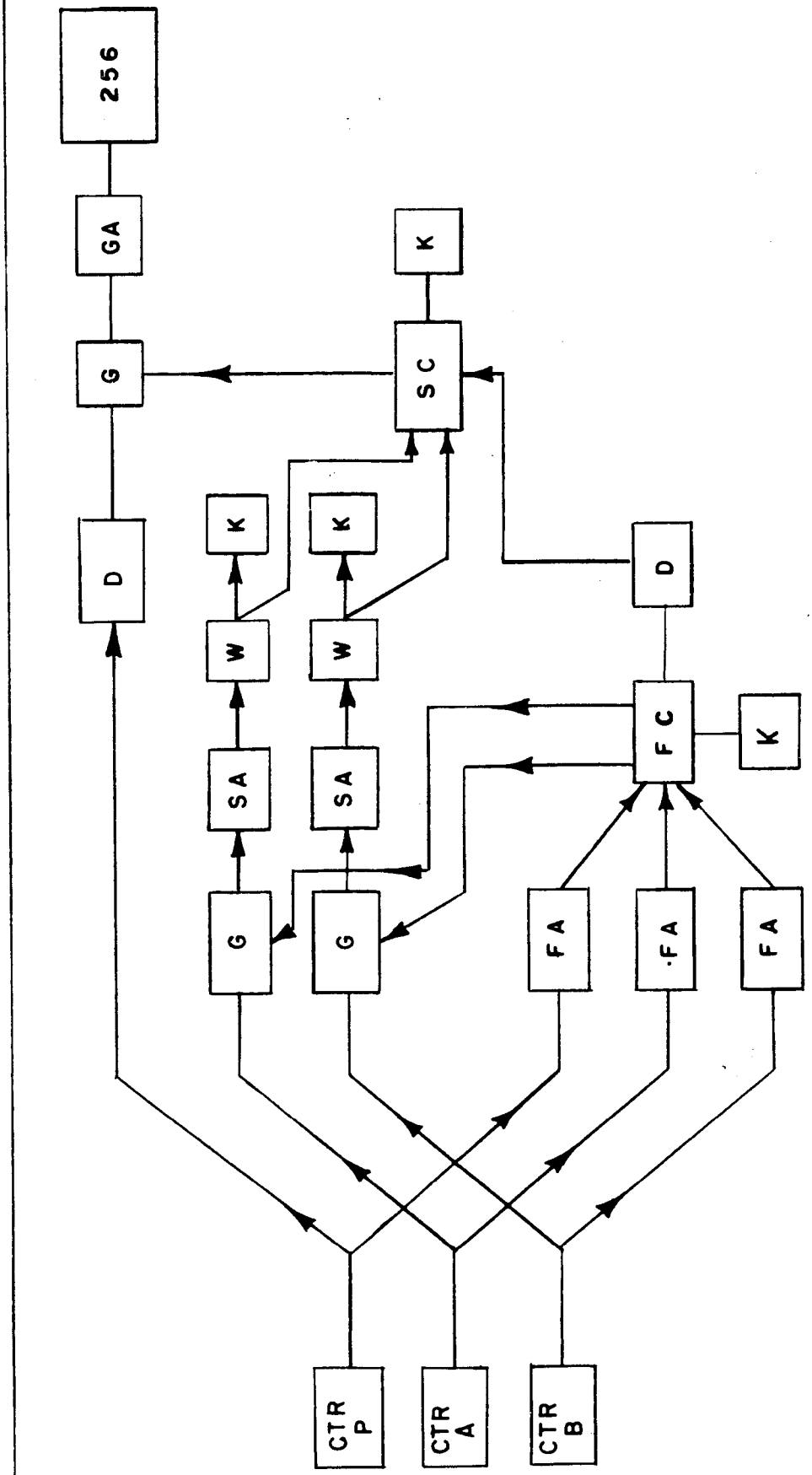

F = FAST S = SLOW A = AMPLIFIER C = COINCIDENCE CKT. D = DELAY G = GATE

K = SCALER 256 = MULTICHANNEL ANALYZER W = SINGLE CHANNEL DISCRIMINATOR

Figure 7. Block diagram of 3-crystal spectrometer and electronics.

Upon placing the spectrometer in the position shown in Figure 8, a steady increase in gain was observed. A graph showing this gain change is shown in Figure 9. A sharp change in the gain of

Experimental Geometry

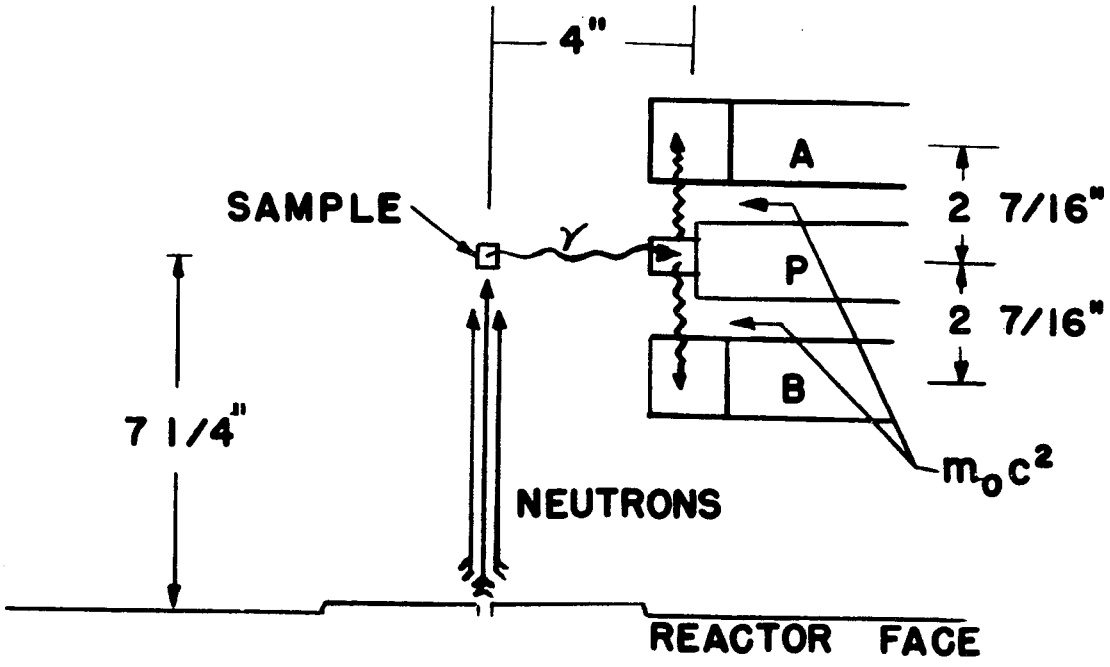

Figure 8. Experimental geometry of the 3-crystal spectrometer.

photomultipliers immersed in a strong gamma-radiation field has been observed[57]. Other reactor experiments on neutron-capture radiation have also been troubled by similiar drifts[58]. Investigation indicated that fast neutrons and poor phototubes were the major contributors to the problem. Thus, by wrapping new phototubes in cadmium and encasing the spectrometer in three inches of lithium-impregnated paraffin, the drift was minimized.

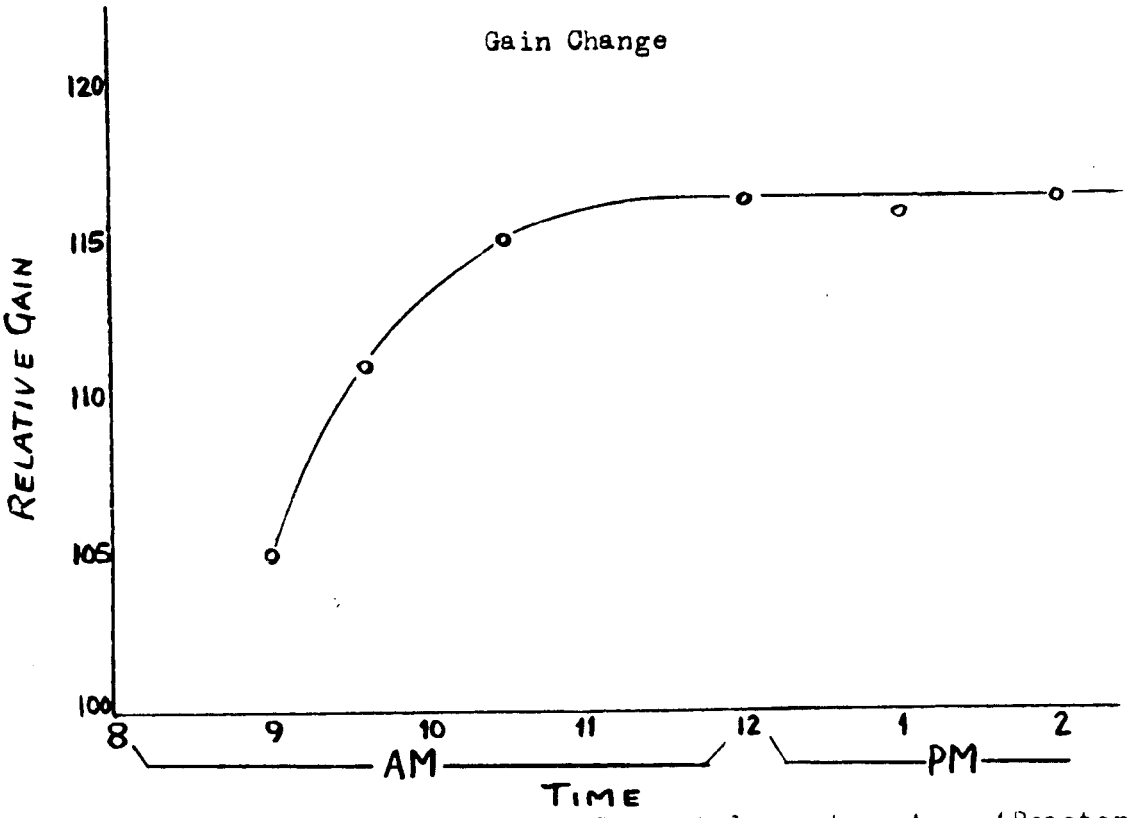

Figure 9. Gain change of the 3-crystal spectrometer. (Reactor on at 8:45 AM.)

The efficiency of the three-crystal spectrometer was determined by taking the average of two estimations of the relative efficiency, and normalizing to a direct measurement of the efficiency made at 2.75 Mev, using a Na^{24} source. The two methods of estimating the relative efficiency of the spectrometer were: (a) by calculation of the relative intensity of the pair production process in the primary crystal, from known cross sections of NaI, assuming that the fraction of two escape processes were independent of the incident photon energy - this calculation is represented by the open points in Figure 10; (b) by measuring the relative intensities of the chlorine (n, γ) spectrum and comparing with the results of

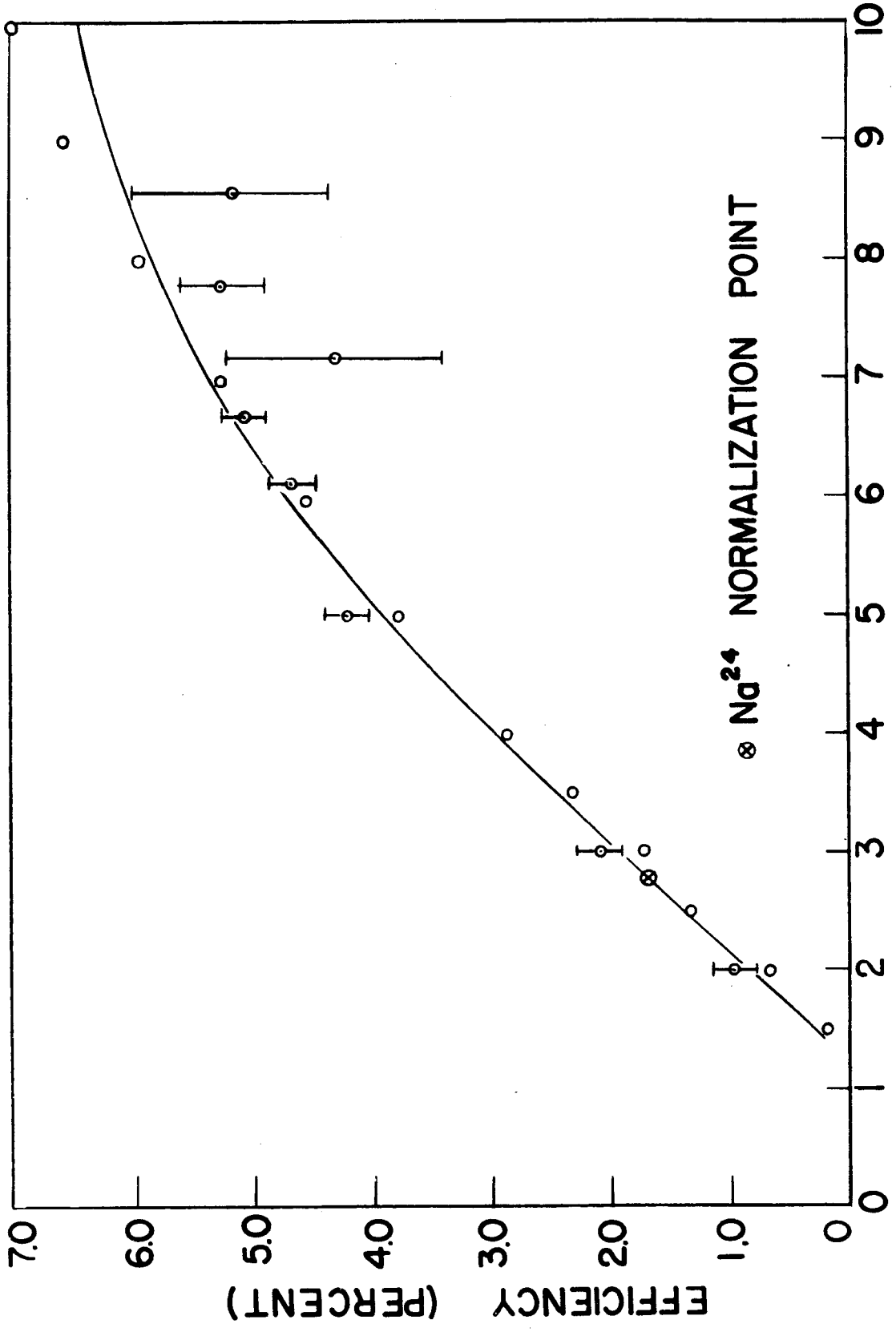

Figure 10. Efficiency of 3-crystal spectrometer.

Groshev et al.[59] - these are the solid points in Figure 10. The two relative efficiency curves were then fitted to each other, averaged, and normalized to give the curve shown in Figure 10. The accuracy attributed to the final efficiency curve varied from ± 10% near the normalization point to ± 25% at the high energies.

The energy resolution of the three-crystal spectrometer was measured to be 2.9% at 6.8 Mev and 5.5% at 2.75 Mev by using gamma rays from $Ni^{62}(n,\gamma)Ni^{63}$ and the radioactive decay of Na^{24}, respectively. The mono-energetic line shape of the spectrometer was approximately independent of energy. A spectrum of Na^{24} taken with this instrument is shown in Figure 11.

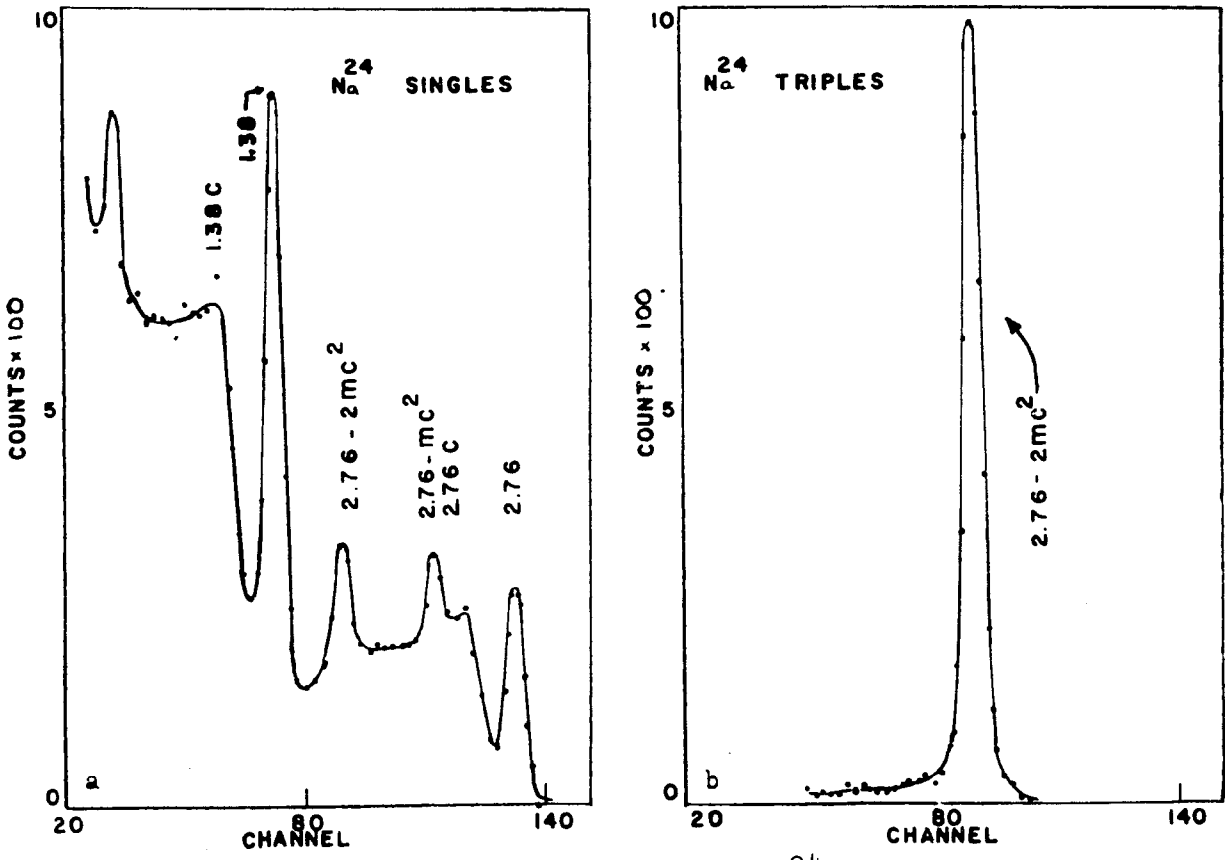

Figure 11. (a) Singles spectrum of a Na^{24} source. (b) Spectrum of the same source taken with the 3-crystal spectrometer.

The energy resolution of the single crystal was measured to be 10.1% at 0.662 Mev. Because the intensity of the low-energy gamma rays could not be obtained due to the tremendous low-energy background of the experiment, the efficiency of the single crystal was not determined.

CHAPTER IV

PROCEDURE

A. Spectra Accumulation and Analysis

Most spectra were measured over a period of a few days. It was necessary, therefore, to adjust the electronics periodically. Each day, prior to reactor operation, three adjustments were made: (a) The gains of the side counters in the spectrometer were made equal. (b) The side counter discriminators were set over the annihilation peak, keeping the base-line and window-width approximately constant. (c) The fast amplifiers of the side counters were adjusted to allow pulses corresponding to gamma rays of energy $\gtrsim$ 475 kev to fire the fast coincidence circuit. After about three hours of reactor operation, when the gain stabilized, two more adjustments were made with a chlorine sample in the beam: (a) The fast-coincidence discriminator was adjusted to keep the coincidence counting rate constant. (b) The side counter discriminators were reset over the annihilation peak.

Samples were then placed in the neutron beam by means of an HO-gauge model electric train, and spectra measured. In most cases, spectra were measured using energy analysis on only one side counter. There was no visible change in the spectra if only one side counter was analyzed.

To insure proper spectrum accumulation, the electronics was

monitored throughout each run. The fast-coincidence, gate-trigger, and scattered-neutron counting rates were monitored and various pulses were periodically observed on an oscilloscope. To minimize the effect of small electronic drifts, the energy scale of each spectrum was adjusted according to a calibration curve obtained from a chlorine spectrum such as the one shown in Figure 12, which was taken after every second spectrum of the sample being investigated.

The fitted spectra were added together and the background was subtracted to give the true spectrum. The background will be discussed in the next section of this chapter. The energies of the gamma-ray lines observed with each sample were determined from a scale based on the energies of the chlorine capture gamma rays given by Groshev et al.[59]. Typical chlorine spectra observed with the three-crystal and single-crystal spectrometers are shown in Figures 12 and 13. The intensities were calculated using the efficiency of the three-crystal spectrometer, the neutron-capture cross sections of the sample and the number of gamma rays observed in a line, which was determined by sketching the known line shape of the spectrometer under each peak and measuring the area of the line with a planimeter.

When samples of separated isotopes were investigated, a gamma ray was assigned to a particular isotope if: (a) it had an energy corresponding to a gamma ray observed with a sample of the natural element, and (b) the counting rate in the peak exceeded that in the valley by at least 3 times the standard deviation. In the

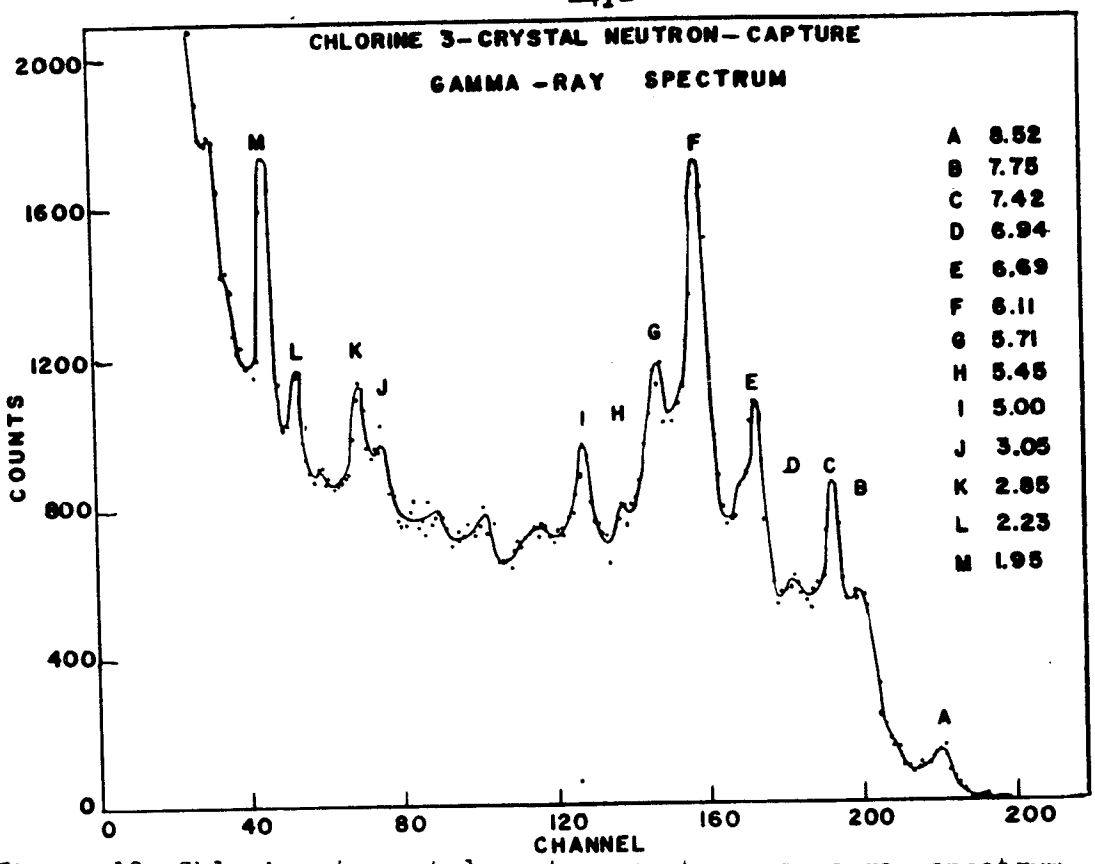

Figure 12. Chlorine 3-crystal neutron-capture gamma-ray spectrum.

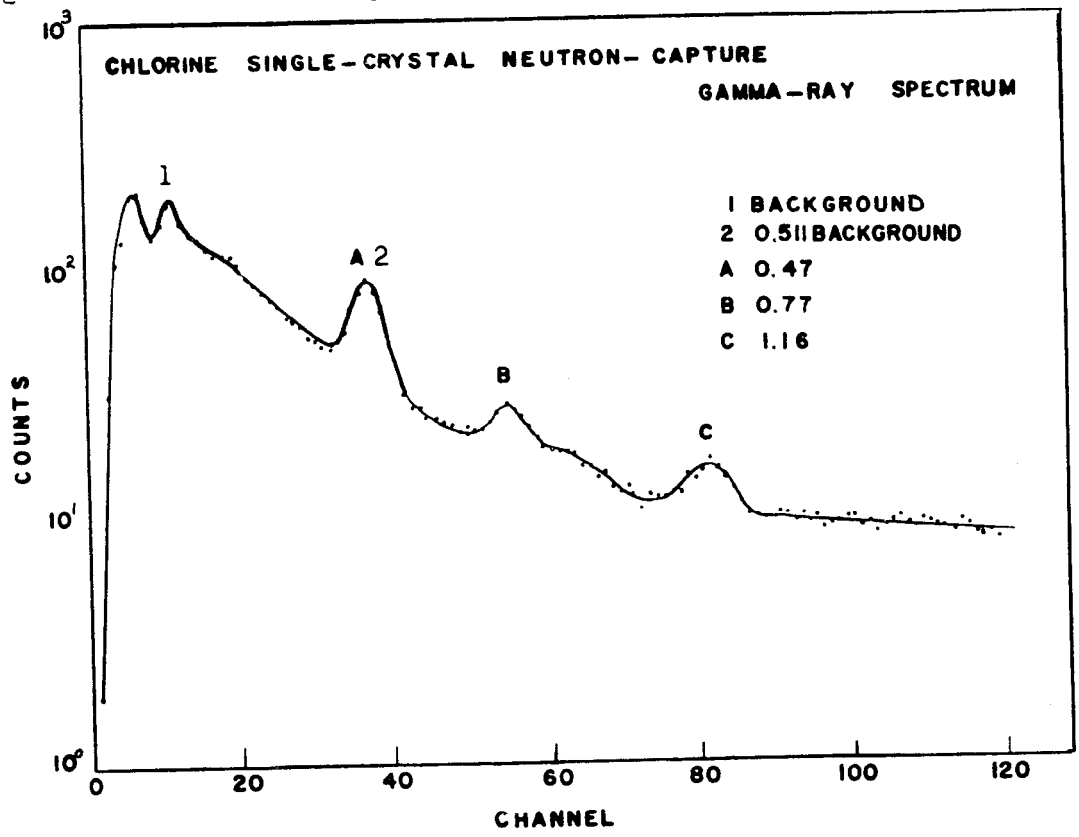

Figure 13. Chlorine single-crystal neutron-capture gamma-ray spectrum.

investigation of nickel, whenever two isotopes seemed to have the same gamma-ray energy, data from $Ni^{58}(d,p)Ni^{59}$ and $Ni^{60}(d,p)Ni^{61}$ were consulted. If a level existed there which was compatible with the energy of the gamma ray, the assignment was made in agreement with the (d,p) data. A few gamma rays of natural copper were assigned to either Cu^{64} or Cu^{66} by consulting data from $Cu^{63}(d,p)Cu^{64}$ and $Cu^{65}(d,p)Cu^{66}$.

The highest energy gamma ray of any isotope was assumed to be its ground state decay; hence, its neutron binding energy. In all cases the relative intensity of the highest energy gamma ray was in qualitative agreement with the possible spin changes for a ground state transition. Total-coincidence spectra were measured with the isotopically enriched samples, and were consulted in determining the neutron binding energy. In a total-coincidence spectrum, the relative intensity of the gamma ray corresponding to the ground state transition was less than in a three-crystal spectrum. To determine the binding energies of the products of natural samples, data from the investigations of (d,p) reactions and mass spectroscopic measurements, as well as calculations using the Weizsäcker mass formula, were consulted.

The errors in this experiment were attributed to various factors. The uncertainties quoted for the energy measurements, $\lesssim 3\%$, depended on the resolution of the spectrometer, the complexity of the spectrum, and the stability of the electronics. The uncertainties in

the intensities also included three components: an uncertainty of 10-20% in determining the area under each peak, 10-25% in the spectrometer efficiency, and 30% in beam intensity, geometry and published cross sections. The error flags on the spectra represent statistical errors only.

B. Background Corrections

There was an appreciable background contribution to all spectra obtained in this research. The background for any sample had four components:

1. Direct reactor gamma rays which were Compton scattered from the sample.
2. Neutron-capture gamma rays from the internal and external shielding which were Compton scattered by the sample.
3. Neutron-capture gamma rays of the external shielding which reached the spectrometer directly.
4. Radioactive gamma rays from the neutron activation of the primary NaI crystal of the spectrometer.

The fourth component was observed only after the reactor had been shut down; therefore, it was assumed to be negligible.

For any spectra, the counts observed at any energy, E_γ, could be expressed as:

$$C_S = X_S(E_\gamma)I(E_\gamma) + Y_S(E_\gamma)F + D(E_\gamma) + Z_S B(E_\gamma)$$

where $X(E_\gamma) \cdot I(E_\gamma)$ was due to Compton scattering of gamma rays in the sample, $Y(E_\gamma)F$ was the true neutron-capture gamma-ray contribution to the counts, $D(E_\gamma)$ was due to gamma rays which reached the

spectrometer directly when no sample was in place, and $\Sigma B(E_\gamma)$ was due to neutrons scattering from the sample and causing (n, γ) reactions in the external shielding and spectrometer. X_s, Y_s and Z_s depended on the sample material, while X_s, Y_s, I, D, and B were functions of the gamma-ray energy, E. F is a constant and is the capture-neutron flux.

X_s, Y_s and Z_s were calculable from the experimental geometry and known cross sections of the samples investigated[60-62]. Knowing X_s, Y_s, and Z_s, I, F, D and B were determined by using four samples of different material and by measuring C_s for each sample. Lead, aluminum and water, which have low-intensity capture gamma-ray spectra[59], were used to evaluate I, F and B, while D was the measured C_s with no sample in place. These parameters are given in Table III.

Table III

Background Parameters

Mev	I	$Bx10^4$	$Dx10^4$
1.5	34.1	199	257
2.0	25.1	84	109
3.0	11.3	37	90
4.0	7.8	38	57
5.0	5.2	26	36
6.0	3.1	18	26
7.0	1.5	12	10
8.0	0.9	7	3
9.0	0.5	4	0
10.0	0.2	2	0

$F = (3.4 \pm 1.5) \times 10^5$ nt/cm^2 sec

Two assumptions were made to facilitate the parameter calculations: (a) The gamma-ray beam was assumed to be parallel to the detector axis. (b) The sample was assumed to be rectangular in shape. By measuring the primary-detector counting rate as a function of sample-to-detector distance d, assumption (a) was proved to be approximately true. Assumption (b) was made because cylindrical and rectangular samples of the same cross-sectional area and total volume produced approximately the same spectra and because it was easier to work with rectangular coordinates.

It was difficult to determine precisely the number of gamma rays of energy E per neutron capture that were emitted by the background samples. However, by comparing previously measured spectra[59], and spectra obtained with the three-crystal spectrometer, good estimates were made of this parameter.

The background parameters obtained were used to calculate a bismuth spectrum, which agree with a measured one within 13% at 3 Mev and 17% at 7 Mev.

The background of any spectrum was obtained by forming

$$K_o = X_o(E_\gamma)I(E_\gamma) + Z_o B(E_\gamma) + D(E_\gamma)$$

and multiplying it by two correction factors. These were to correct for any changes which occurred between the time the background was obtained and the spectrum measured. The first corrected for any change in relative window-width of the side counter and the second corrected for any gain change of the spectrometer.

In Figure 14 are shown the three components of the background for Ni^{62}, corrected individually.

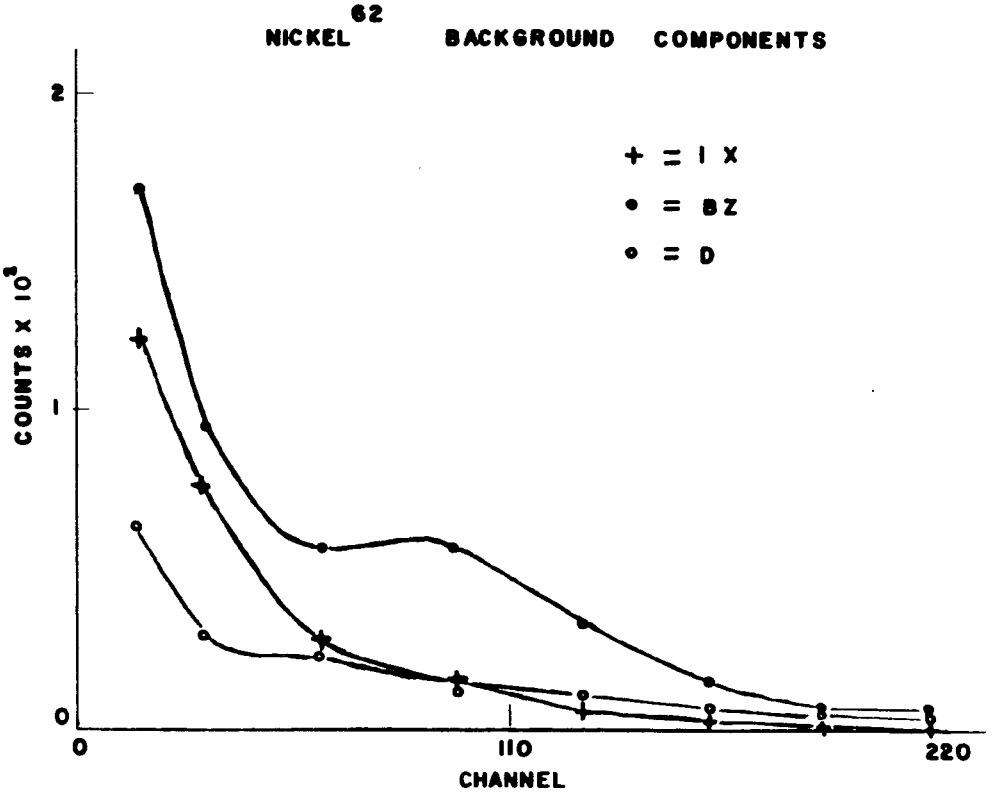

Figure 14. The three components of the Nickel 62 background.

These were added together to give the spectrum of Figure 15, which is a typical background spectrum. The peaks that are shown were due to hydrogen, bismuth, lithium and lead. These peaks were sketched in with a peak to valley ratio that is constant in all the measured background spectra.

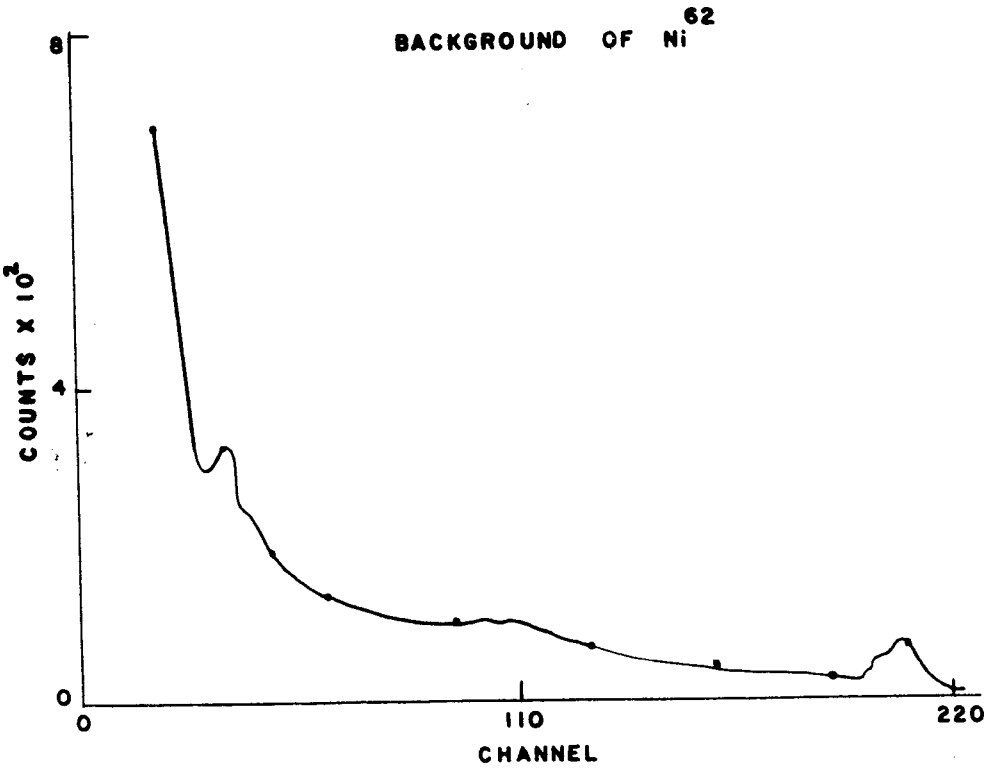

Figure 15. Nickel 62 3-crystal background spectrum.

CHAPTER V

RESULTS

A. Bromine Isotopes

The gamma-ray spectrum following thermal-neutron capture in natural bromine has been investigated by Campion and Bartholomew[63], using an external conversion spectrometer and a large mass of target material. In the present work, 2.5 gram samples of ammonium bromide, whose constitutions are indicated in Table IV, were irradiated in the neutron beam.

TABLE IV

Isotopic constitution of the bromine samples. The chemical impurities in each sample were less than 0.05%.

Sample (nominal)	Mass (grams)	Constitution (%) Br^{79}	Br^{81}
Natural	2.56	50.6	49.4
Br^{79}	2.74	95.1	4.9
Br^{81}	3.21	8.3	91.7

The three-crystal spectra were measured over a period of three months, with each spectrum being accumulated for four hours on the 256-channel analyser. They are shown in Figures 16a, 16b, and 16c. The single-crystal spectra were measured for five minutes on three operating days. The spectra with background substracted are shown in Figures 17a, 17b, and 17c. The total-coincidence spectra are

shown in Figures 18a and 18b, along with the three-crystal spectra obtained with no side-counter energy analysis.

TABLE V

Energies (E_γ) in Mev and intensities (I_γ), in photons per 100 captures in the individual isotope, of the neutron-capture gamma rays from separated bromine isotopes. Uncertainty in the last given digit is indicated in parentheses.

	Present Results					Campion et al.	
Key	Natural Br	Br^{80}		Br^{82}		Natural Br	
	E_γ	E_γ	I_γ	E_γ	I_γ	E_γ	I_γ
						7.88	0.2
						7.78	0.2
a	7.62	7.63(8)	.5(.3)	7.62(8)	1(.7)	7.58	1.6
b	7.30+			7.30 (9)+		7.17	0.7
c	7.03	7.04(9)	.8(.5)			7.05	1.0
d	6.72	6.67(8)	.7(.5)	6.65*(9)		6.72	1.0
e	6.06*	5.95*(8)		6.06(8)	1.2(.7)	6.11	1.1
f	5.64			5.65(8)			
g		5.00(8)					
h	4.77			4.75(8)			
i		4.47(8)+		4.47(8)+			
j	4.00	4.03(8)					
k	3.50+						
β	5.47	5.30(8)		5.47(8)			
A	1.14(8)(?)						
B	0.36(5)(?)						
C		0.19(4)(?)					

*Unresolved group of lines.

+ Strong N^{14} $(n,\gamma)N^{15}$ line of this energy exists (See text).

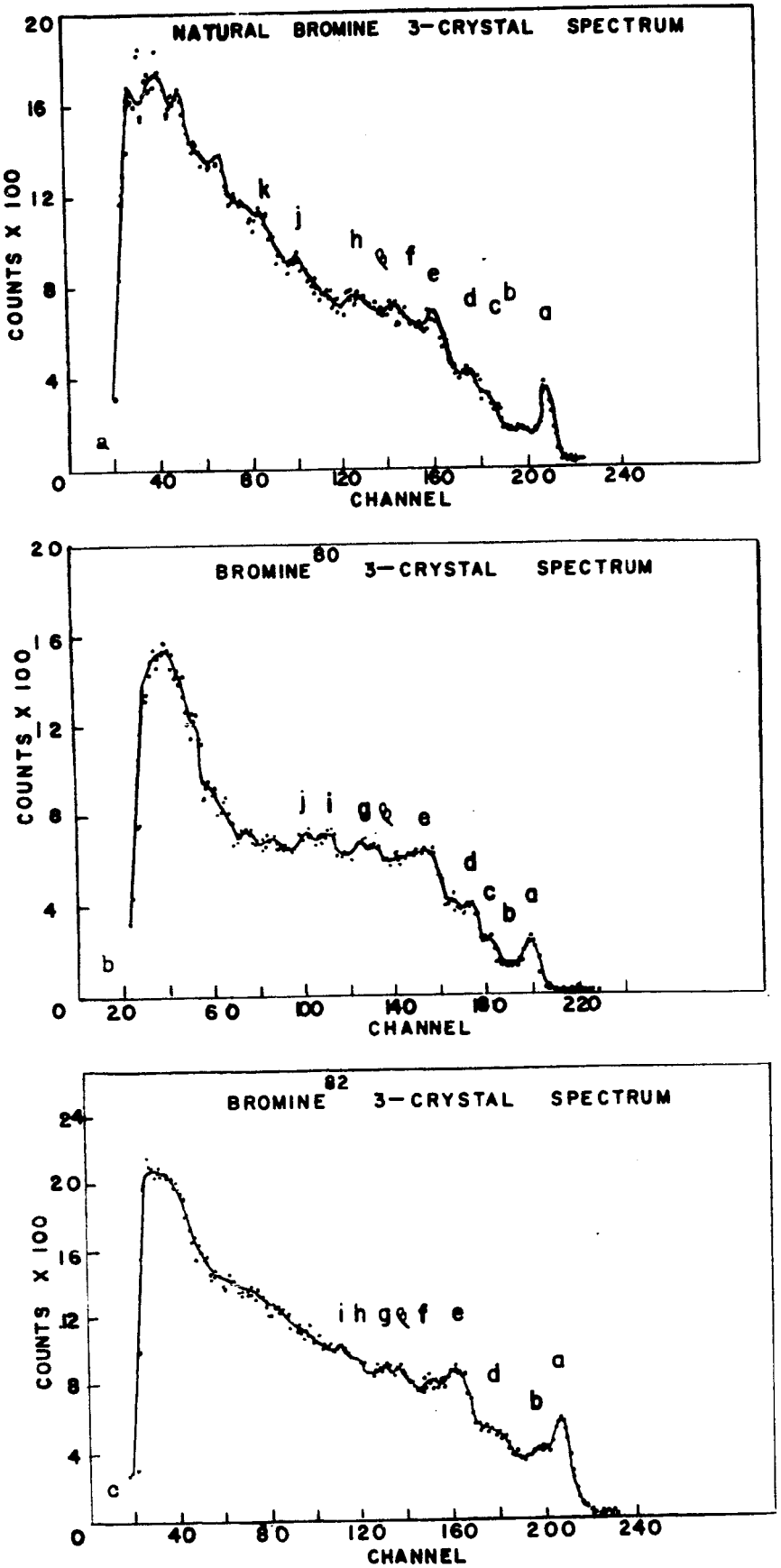

Figure 16. 3-crystal neutron-capture gamma-ray spectra of (a) Natural Bromine, (b) Bromine 80, and (c) Bromine 82.

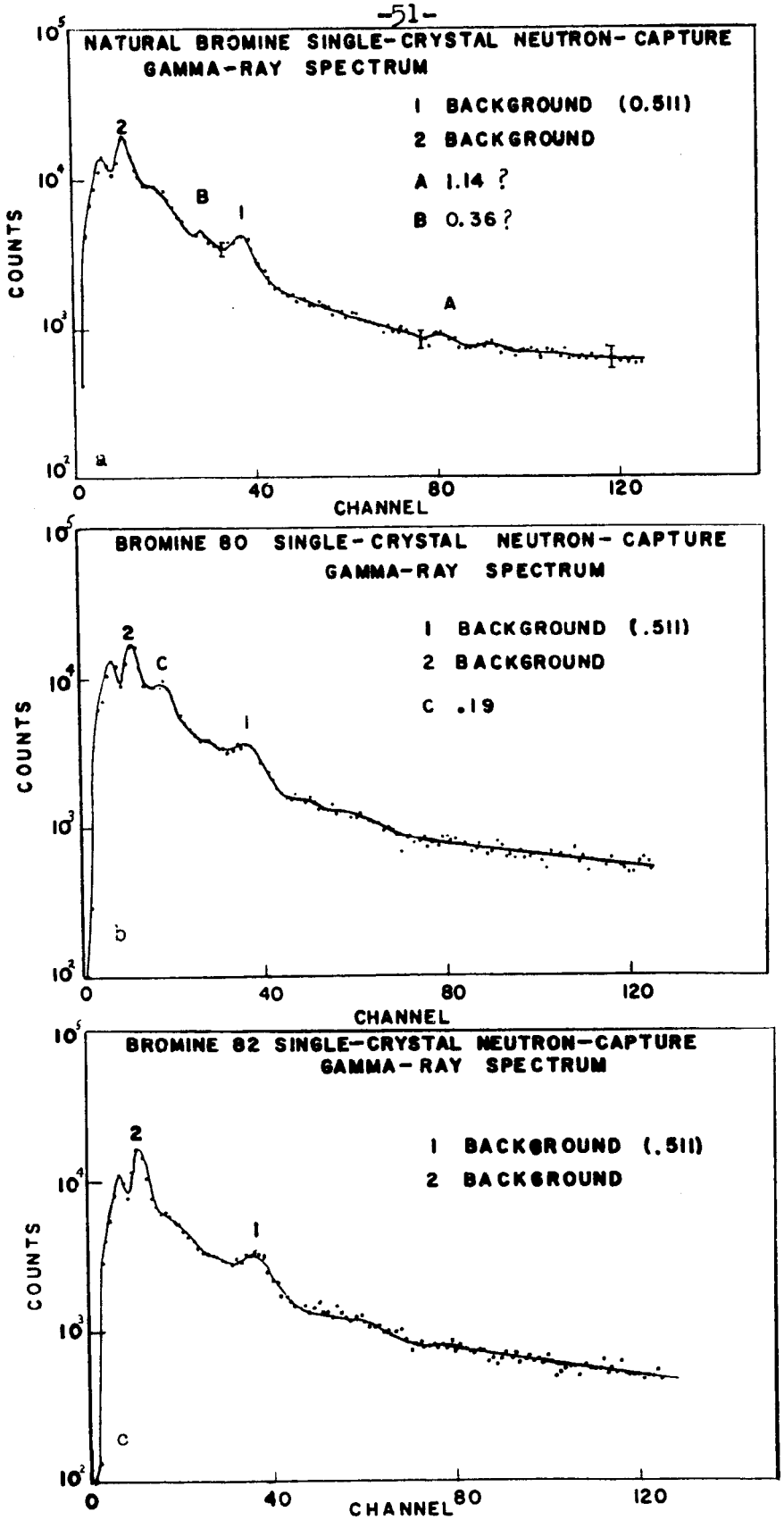

Figure 17. Single-crystal neutron-capture gamma-ray spectra of (a) Natural Bromine, (b) Bromine 80, and (c) Bromine 82

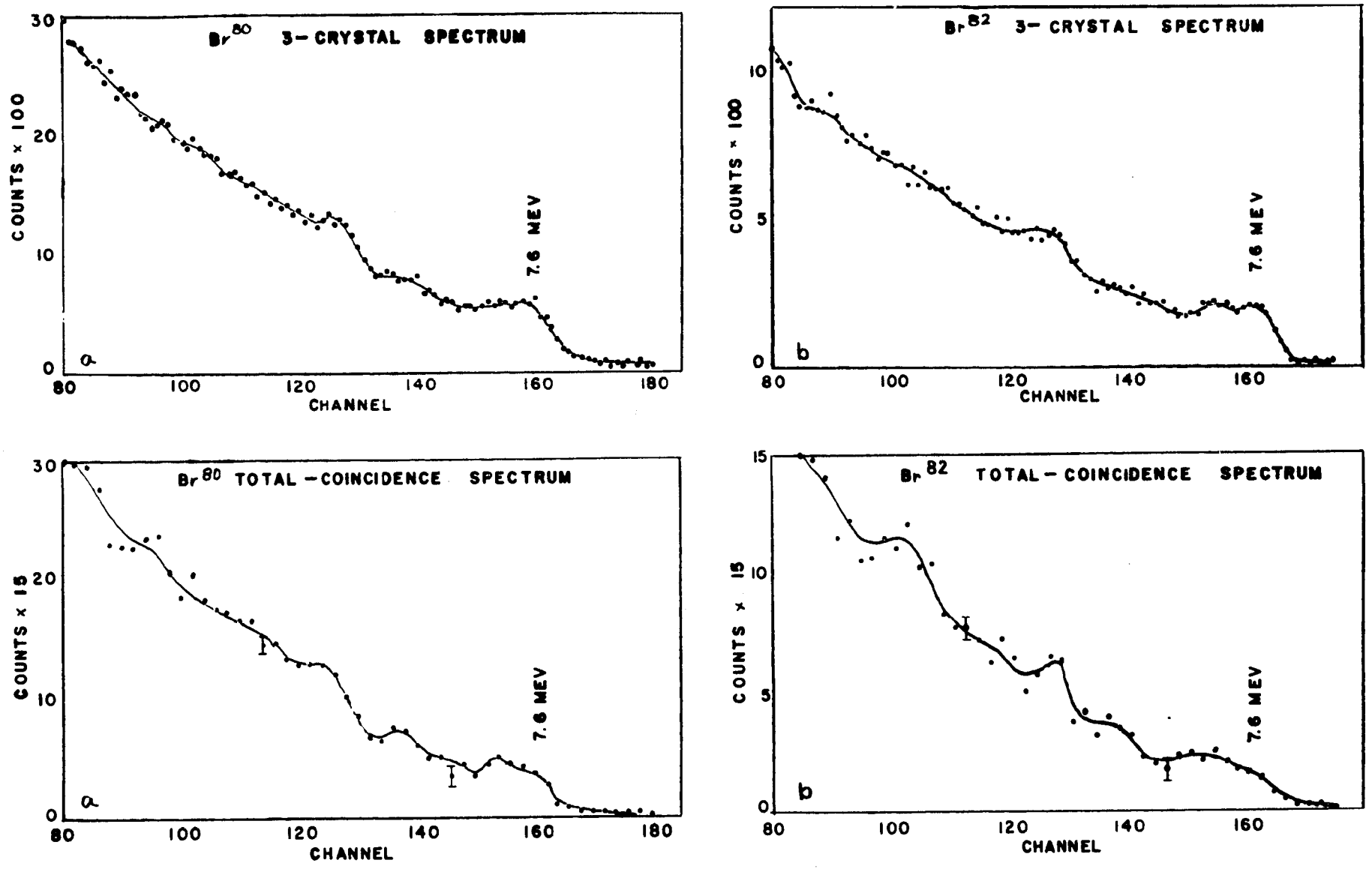

Figure 18. Total-coincidence spectra of a BROMINE 80 and b BROMINE 82.

The gamma ray energies and the intensities, per 100 neutrons captured, of the high energy gamma rays, taken from Figures 16a - 17c, are listed in Table V. Gamma rays were included in Table V if their peak-to-valley height was at least equal to the statistical fluctuations. The intensities were calculated using a neutron-capture cross section of 2.9 and 2.6 barns for Br^{79} and Br^{81}, respectively, and assuming the capture-neutron beam to be $(3.4 \pm 1.2) \times 10^5$ neutrons per cm^2 per sec.

The intensities of only a few gamma rays were determined because the spectra were very complex and because the nitrogen in the samples contributed some lines to the spectrum. The cross section for neutron capture in nitrogen is only 90 mb, but the intensity of many of the nitrogen capture gamma rays exceeds 15. Consequently the gamma rays at 7.30, 4.52, and 3.46 Mev were attributed to N^{15}.

The spectra suggested that the neutron binding energies were 7.62 Mev for both Br^{80} and Br^{82}. They were calculated to be 7.1 and 6.4 Mev, respectively, by Martin[64], and 7.89 and 7.65 Mev by Wapstra et al.[65]. Because the highest energy gamma rays, 7.62 Mev, were only slightly depressed in the total-coincidence spectra, there was no clear indication that the 7.62 Mev gamma rays were the ground state transitions. Furthermore, as stated in the Appendix, the spins of the capture states and ground states of Br^{80} are 1^+ or 2^+ and 1^+, and of Br^{82} are 1^- or 2^- and 5^+. Hence, only Br^{80} should have had a relatively strong ground state transition. The 7.62 Mev gamma ray of

Br^{82} could have been a decay to an excited state, but no strong low-energy lines were observed from Br^{82}. Thus, the suggestion that the binding energy of both Br^{80} and Br^{82} is 7.62 Mev is not consistent with the calculated binding energies or the spins of the capture and ground states.

The bromine nuclei studied were odd-odd, and their spectra were extremely complex, as expected. The general shape of their spectra was similar to that generated by a level density $\rho = \rho_0 e^{\sqrt{\alpha E}}$ with $\alpha = 5\ \text{Mev}^{-1}$ and implied that these nuclei would be best represented by a shell model. No lines were intense enough to imply an appreciable direct capture or anomalous resonance capture cross section for either Br^{79} or Br^{81}.

B. Natural Copper

The gamma-ray spectrum following neutron capture in natural copper has been investigated by Groshev et al.[59], Bartholomew et al.[66], and Reier[21], using external conversion magnetic spectrometers, and by Sklyarevskii et al.[67], using a single scintillation crystal and separated isotopes of Cu^{63} and Cu^{65}. They found a relatively complex spectrum, but were able to assign many gamma-ray energies. Buechner et al.[68] recently investigated the reactions $Cu^{63}(d,p)Cu^{64}$ and $Cu^{65}(d,p)Cu^{66}$, while Trumpy[30] investigated the circular polarization of gamma rays following polarized neutron capture in natural copper. It was hoped that by coupling all previous data with the measurements of the present research, a more realistic decay scheme for the two copper isotopes Cu^{64} and Cu^{66} could be proposed, and the neutron binding energies determined. However, only the binding energies were determined.

A 14 gram sample of metallic copper powder, which contained both Cu^{63} and Cu^{65}, was placed in the beam, and the three-crystal copper spectra were measured over a period of three fifteen-hour days, with each spectrum being accumulated for four hours. The fitted copper spectra were added together and the background was subtracted to give the spectrum shown in Figure 19. The single-crystal spectra were measured for five minutes on three different operating days. A single-crystal spectrum is shown in Figure 20.

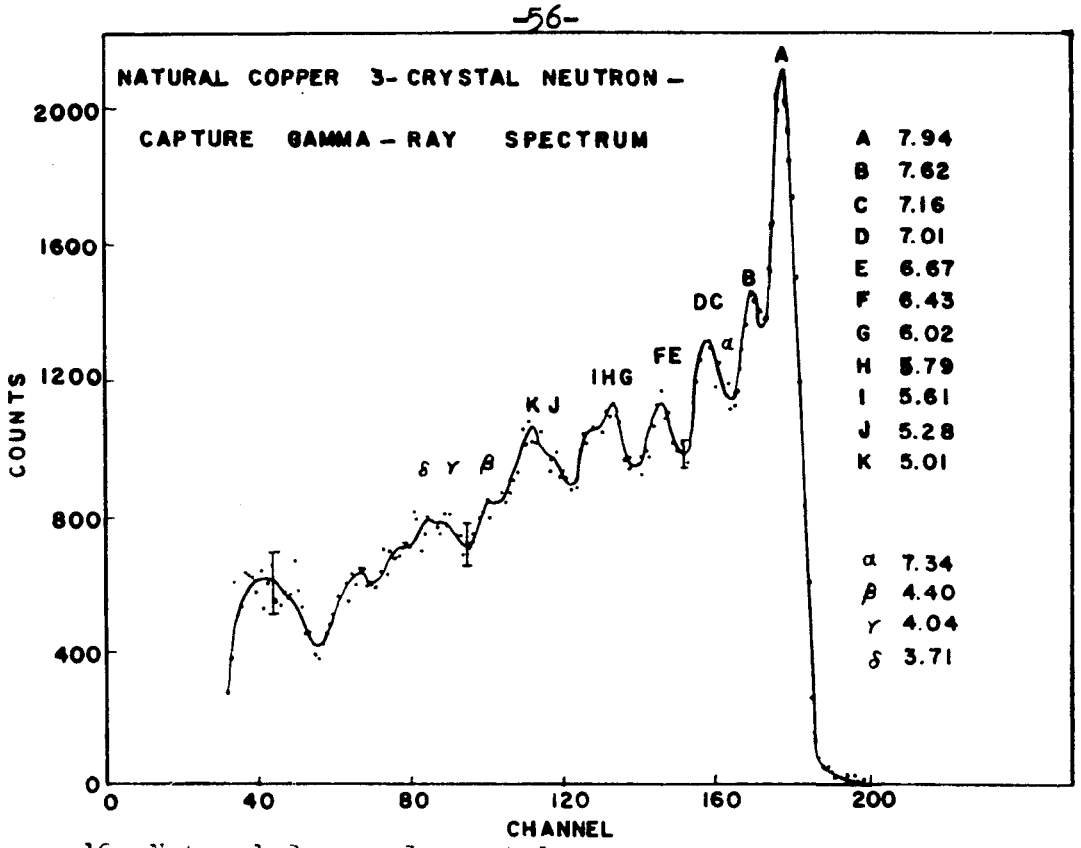

Figure 19. Natural Copper 3-crystal neutron-capture gamma-ray spectrum

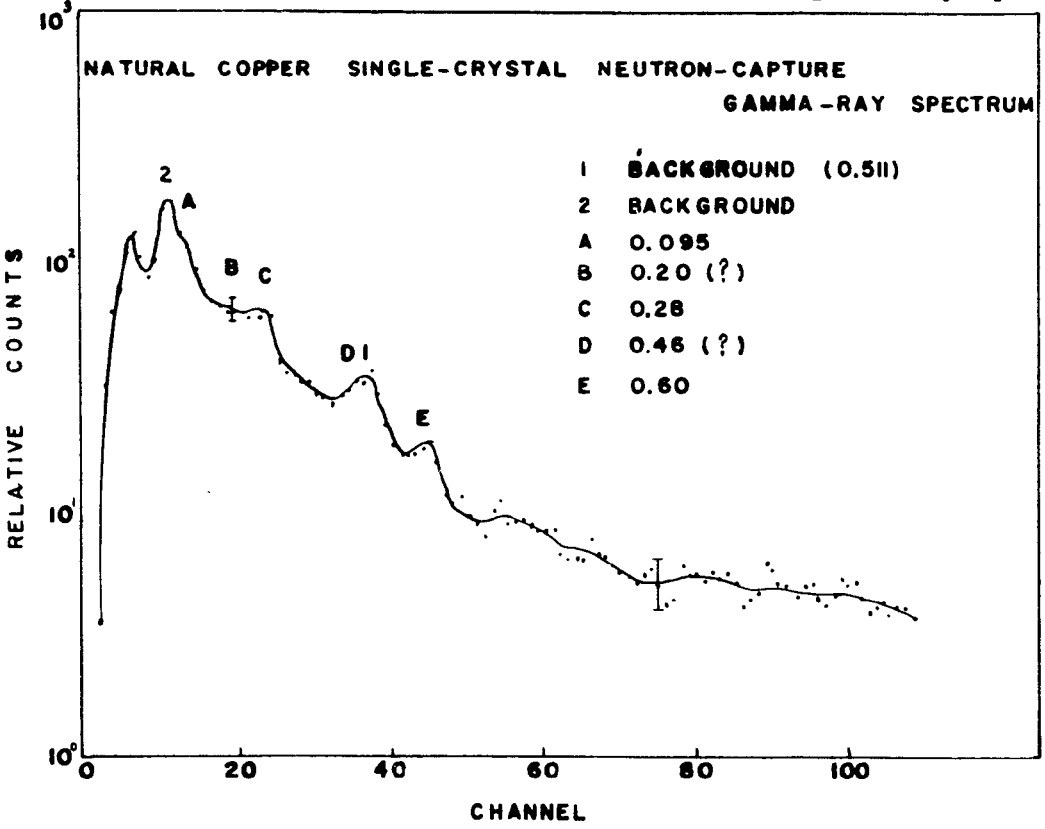

Figure 20. Natural Copper single-crystal neutron-capture gamma-ray spectrum.

The gamma-ray energies and the intensities per 100 neutrons captured of the high energy gamma rays, taken from Figures 19 and 20, are listed in Table VI. The energy scale was based on the energies of the chlorine capture gamma rays of Groshev et al.[59]. The intensities were calculated using a neutron capture cross section of 3.6 barns.

Natural copper and its isotopes have been studied by various techniques such as (d,p) reaction, the radioactive decay of neighboring nuclei and mass spectroscopy. The Q values and the corresponding neutron-binding energies are given in Table VII, as are the mass spectroscopic values for the binding energies obtained by K. S. Quisenberry et al.[69], and the values given by Wapstra et al.[65]. For both Cu^{64} and Cu^{66} the ground state has J=1 , while the capture state has $J=1^-$ or 2^-. This implies that a strong ground state transition should have been observed for each isotope. Intense gamma rays, corresponding to the above binding energies, were observed at 7.94 and 7.01 Mev and were presumed to be the ground state decays. A few of the gamma rays observed correspond to transitions observed in (d,p) experiments. The gamma rays and corresponding (d,p) proton groups are listed in Table VIII.

Because of the intense high-energy gamma rays, the copper spectrum could not be compared to those predicted from a statistical model. This strong group of high-energy transitions implied that direct capture and anomalous resonance capture contributed to the neutron-capture cross section. Lane and Lynn[44], calculated the direct

TABLE VI

Gamma ray energies and intensities of Natural Copper

	Present Results		Bartholomew[a] et al.		Groshev[b] et al.		Trumpy[c]	Reier[d]	Sklyarevskii[e] et al.
Key	E	I	E	I	E	I	E	E	E
a	7.94(4)	22(9)	7.91	20	7.91	22			
b	7.62(6)	12(7)	7.63	9	7.63	11			
	7.34(10)*		7.30	5	7.29	8			
c	7.16(6)	4(3)	7.16	1	7.14	4			
d	7.01(6)	7(4)	7.01	2	7.00	3			
e	6.67(10)	3(2)	6.69	3	6.63	4			
f	6.43(10)	5(3)	6.41	1	6.39	0.7			
g	6.02(10)	4(3)	6.05	1	6.04	1.2			
h	5.79(10)	4(3)	5.75	0.2	5.77	0.2			
i	5.61(10)	4(3)	5.64	0.5	5.61	0.7			
			5.43	1	5.42	1.9			
j	5.28(12)	4(3)	5.31	1	5.28	2.3			
k	5.01(12)	4(3)	5.18	0.6	5.17	1.1			
			5.07	0.7	5.05	1.1			
					4.75	0.3			
					4.67	0.7			
					4.51	1.1			
	4.40(12)*				4.36	1.5			
	4.04(10)*				4.36	1.5			
	3.71(10)*								
					3.44	0.5			
					3.11	0.7			
					2.65	0.7			
E	0.60						.60		
D	0.48(?)								
C	0.28						.28	.280	.276
B	0.21(?)							.202	.205
									.180
									.155
A	0.095								.092

* not well resolved

a see reference 66
b see reference 59
c see reference 30
d see reference 21
e see reference 67

TABLE VII

Neutron binding energies

Isotope	Natural Abundance of Capturing Isotope	Neutron Binding Energy			
		Present Results	Buechner[a] et al.	Quisenberry[b] et al.	Wapstra[c] et al.
Cu^{64}	69%	7.94	7.92	7.92	7.92
Cu^{66}	31%	7.01	7.06	7.06	7.06

[a] see reference 68
[b] see reference 69
[c] see reference 65

TABLE VIII

Comparison of capture gamma-ray energies (E_γ) with excitation energies (E_x) from (d,p) reactions in Cu^{64} and Cu^{66}. Assignments are in terms of the product nucleus. Energies are in Mev.

Present Results		(d,p) results[a]	
E_γ	Assignment	E_x	Assignment
7.94	Cu^{64}	7.92	Cu^{64}
7.64		7.64	Cu^{64}
7.18		7.18	Cu^{64}
7.01	Cu^{66}	7.06	Cu^{66}
6.68		6.68	Cu^{66}
6.45		6.45	Cu^{66}

[a] see reference 69

capture cross section for copper to be 0.4 barns. This is approximately 10% of the total capture cross section. Also, they found an enhancement of the average value of the width for a transition from a resonance to a single-particle p-wave state, which would allow anomalous resonance capture. Thus all three capture mechanisms, conventional compound nucleus capture, anomalous resonance capture, and direct capture must have contributed to the capture cross section for copper. It was not possible to determine the relative contributions.

However, it seems apparent that the structure of a capture spectrum depends of the energy distribution of the neutron flux used to measure it, because of the resonance structure of the cross section and the resulting variation in the relative contributions of the three capture mechanisms to the cross section.

C. Natural Iridium

The gamma ray spectrum following neutron capture in Ir^{191} and Ir^{193} has been investigated by Groshev et al.[59] and Knoepfel et al.[70], using external conversion magnetic spectrometers, and Fiebiger[71], using a multi-crystal coincidence spectrometer. They found a very complex spectrum, and were not able to assign energies in the energy region below 5.5 Mev.

Using a 9.7 gram sample of iridium metal powder and accumulating each spectrum on the analyzer for two hours, the iridium spectra were measured over a period of ten eight-hour days. The fitted iridium spectra were added togetner and the background was subtracted to give the spectrum shown in Figure 21. The background was an average of two measurements. One was made by placing in the neutron beam a bismuth sample with a compton scattering capacity equal to that of the iridium sample, and the other was made by using the method described in Chapter IV. The single-crystal spectrum is shown in Figure 22.

The gamma ray energies and their intensities per 100 neutrons captured are listed in Table IX. The intensities were calculated assuming a capture cross section of 460 barns.

Most of the gamma rays present have been reported previously; however, those marked with an asterisk in Figure 21 were observed for the first time in this research. These have the energies 4.32, 4.19,

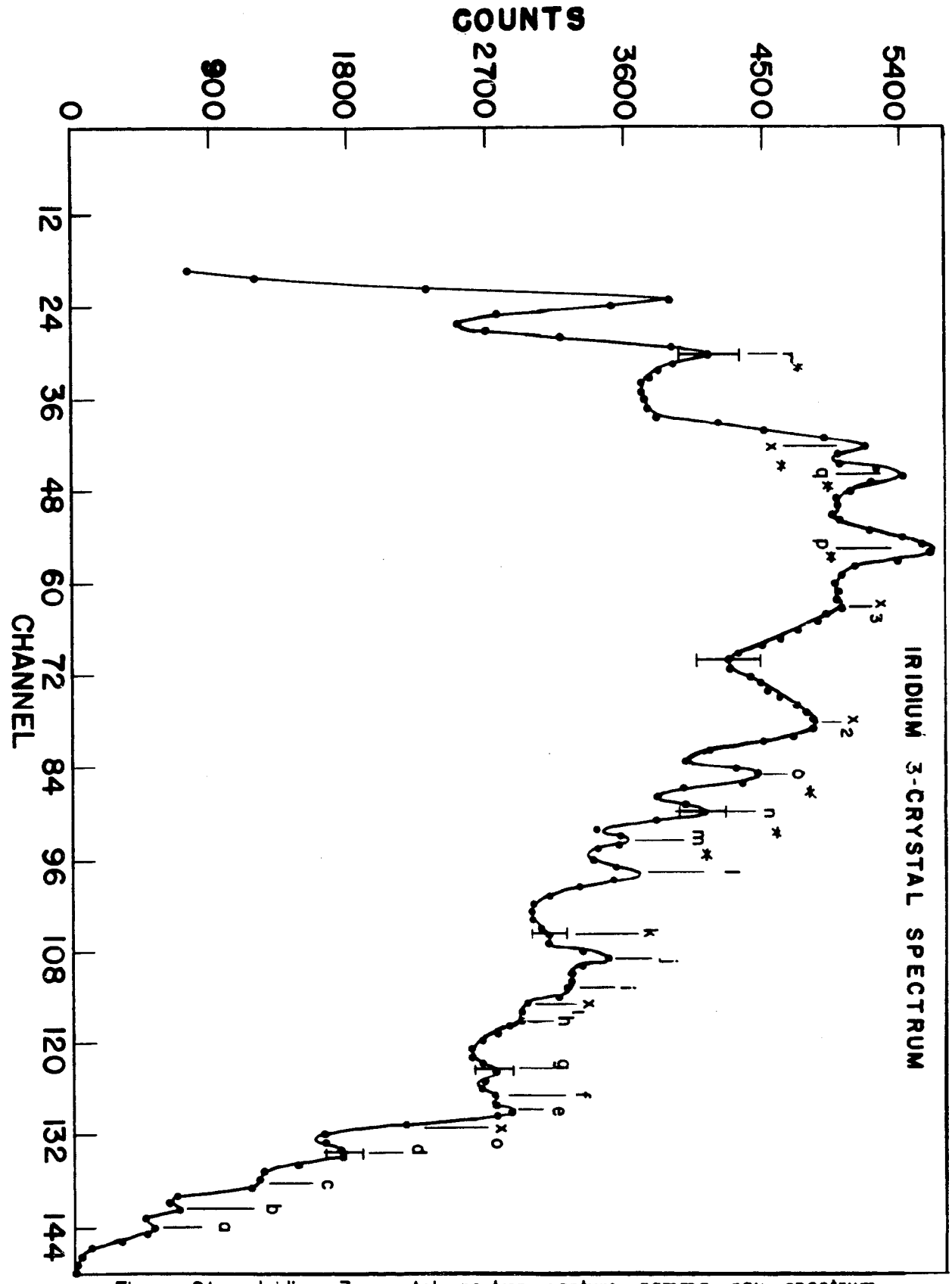

Figure 21. Iridium 3-crystal neutron-capture gamma-ray spectrum.

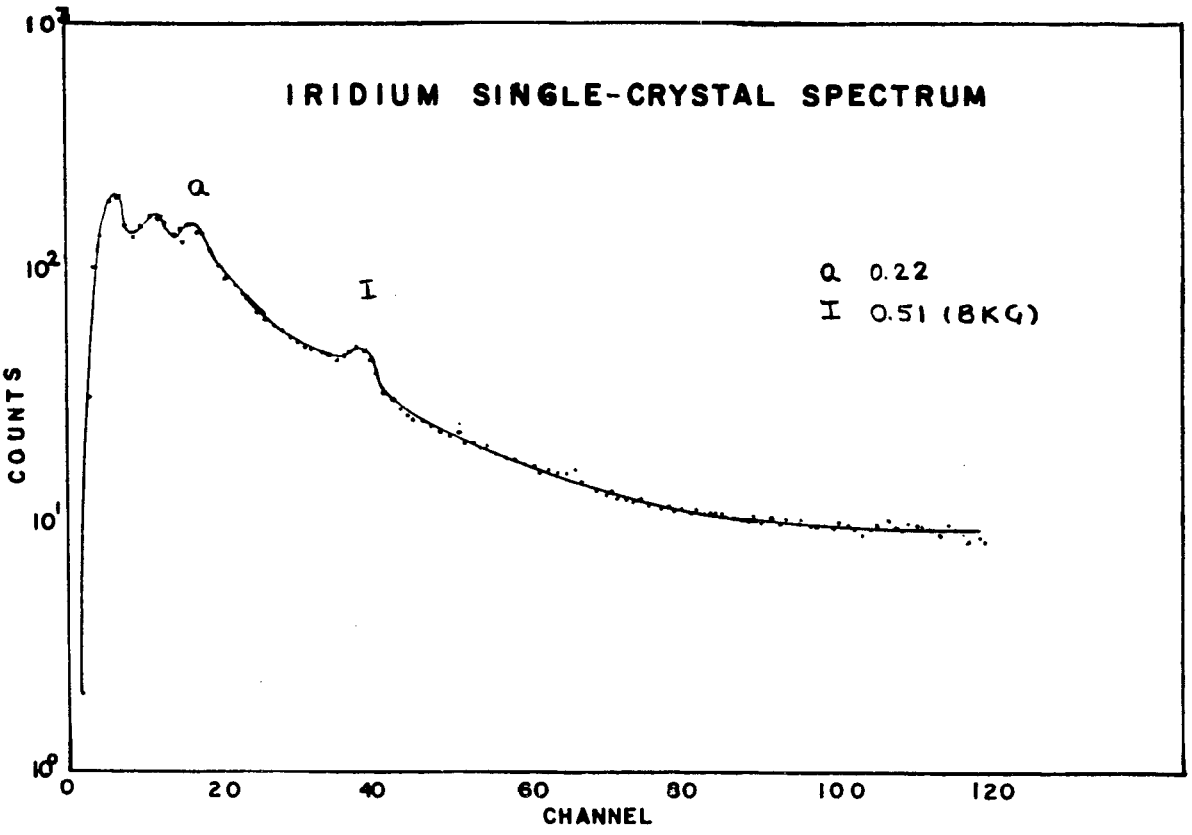

Figure 22. Iridium single-crystal neutron-capture gamma-ray spectrum.

3.97, 2.82, 2.48, and 1.95 Mev. Other gamma rays, which could not be resolved, occurred in the ranges of 3.65 ± 0.20 Mev and 3.15 ± 0.25 Mev. The lines at 5.34 and 5.77 reported by Groshev et al.[59] were not resolved.

TABLE IX

Gamma ray energies and intensities of Natural Iridium

Gamma Ray	Present Results		Groshev et al.[X]		Knoepfel et al.[Y]		Draper[Z]
	Mev	Int	Mev	Int	Mev	Int	Mev
a	6.25						
b	6.17						
c	6.07	0.7(.7)	6.08	0.4	6.08	1.1	
			5.95	0.7	5.97	1.3	
d.	5.90	1.2(.7)			5.92	0.9	
			5.77	0.7			
e.	5.68	2.5(1.3)	5.68	1.5	5.68	1.5	
f.	5.57	1.2(.7)	5.57	1.0	5.57	1.7	
g.	5.45	2.8)2.0)			5.48	1.7	
					5.34		
h.	5.19	1.2(.7)	5.16	0.9			
i.	5.07	2.0(1.2)			5.13		
j.	4.89	4.0(2.0)	4.96	0.8			
k.	4.79	2.5(1.3)			4.79		
					4.60		
l.	4.48	5(2.5)			4.50		
m.	4.32	4(2)					
n.	4.19	4(2)					
o.	3.97	5(3)					
p.	2.82	20(12)					
q.	2.48	22(12)					
r	1.95	25(17)					
x_0	5.77						
x_1	5.34						
x_2	3.75-3.55						
x_3	3.40-3.15						
x_4	2.30						
a	0.22						0.350
							0.215
							0.140

[X] see reference 59; [Y] see reference 70; [Z] see reference 37

Based on mass-spectrometer measurements, Demirkhanov et al.[72], have suggested that the binding energy of a neutron in Ir^{192} and Ir^{194} is 6.24 and 6.14 Mev, respectively. Therefore, the gamma rays a = 6.25 Mev and b = 6.17 Mev of Figure 21 may be the ground state transitions of Ir^{192} and Ir^{194}. This assignment would be in disagreement with Martin[64], who claims the neutron binding energies are 6.08 and 5.95 Mev, respectively. It would also disagree with Fiebiger[71], who suggests that the binding energies could be 6.45 and 6.30 Mev. Martin's binding energies were computed from the Weizsäcker mass formula and Fiebiger's results were ambiguous; consequently, the direct mass measurement is probably the most reliable. Gamma rays a and b are probably the ground state transitions.

It should also be noted that there exists a 0.054 Mev isomeric state in radioactive Ir^{192}. Thus the 6.17 Mev capture gamma ray may be a transition from the 6.25 level to the 0.054 level of radioactive Ir^{192}.

Assuming the above binding energies to be 6.25 and 6.17 Mev, there exist some pairs of observed gamma rays which add up to the neutron binding energies. They are: (4.19 + 1.95), (3.97 + 2.32), 3.75 + 2.48). The many gamma rays above 4 Mev would imply several states below 2 Mev which have not been observed, because the single-crystal spectrum is too complex.

The products formed with a natural iridium sample in the beam were both odd-odd nuclei. The spectrum was extremely complex, as

expected for odd-odd nuclei, but there were a few weak gamma rays observed. Lane and Lynn[44] have calculated the direct capture cross section for iridium to be negligible. The weak lines were probably due to anomalous resonance capture.

The general shape of the spectrum was similar to that generated by $\rho = \rho_0 e^{E/t}$ with $t = 1.0$ Mev. This implied that Ir^{192} and Ir^{194} could be best represented by a collective model level density. Comparing the natural iridium spectrum with that of its neighbor, Pt^{196}, which is an even-even nucleus, a qualitative difference between odd-odd and even-even spectra was observed. Due to the nuclear pairing effect, the upper boundary of the unresolved region in the spectra of even-even nuclei lies approximately 1.4 Mev below the neutron binding energy for the product nucleus, while in odd-odd nuclei these two energies are approximately equal.

D. Nickel Isotopes

Ad'yasevich et al.[32] and Kinsey and Bartholomew[73], using external conversion spectrometers, and T. H. Braid[36], using a Compton scintillation spectrometer, have investigated the capture gamma-ray spectrum of natural nickel. Because these experiments needed large samples, no separated-isotope studies were done. In the present research, natural nickel, in the form of nickel oxide powder, and Ni^{58}, Ni^{60}, and Ni^{62}, in the form of isotopically enriched metallic bars and lumps, were irradiated in the neutron beam. The gamma-ray spectra were detected by means of the single crystal, the three-crystal spectrometer and the total coincidence spectrometer.

The masses and isotopic constitutions of the samples are given in Table X.

TABLE X

Isotopic constitution of the nickel samples. The chemical impurities in each sample were less than 0.05%.

Sample (nominal)	Mass (grams)	Constitution (%) Ni^{58}	Ni^{60}	Ni^{61}	Ni^{62}	Ni^{64}
Natural	7.8	67.8	26.2	1.2	3.7	1.2
Ni^{58}	21.2	99.9	0.06	....	....	....
Ni^{60}	5.4	1.45	98.5	0.02	0.01	....
Ni^{60}	3.0	0.42	0.47	2.8	96.2	0.04

The fitted three-crystal spectra for natural nickel and for each isotope are shown in Figures 23a, 23b, 23c, and 23d. The single-crystal spectra, are shown with background subtracted in Figures 24a,

24b, 24c, and 24d. The total-coincidence spetra of Ni^{59} and Ni^{61} are shown in Figures 25a and 25b.

The energies of the gamma-ray lines observed with the natural nickel sample, in comparison with other recent work, are given in Table XI. The intensities were not measured in this case, but there is good qualitative agreement with other published spectra.

TABLE XI

Energies of neutron-capture gamma rays in natural nickel. The identification letters correspond to those in Figures 23 and 24.

Key	Present results	Kinsey and Bartholomew[a]	Ad'yasevich et al.[b]	Braid[c]
a	8.99(1)	8.997(5)	8.996(10)	
b	8.53(4)	8.532(8)	8.51(3)	
c	8.14(4)	8.119(10)	8.10(3)	
d	7.82(4)	7.817(8)	7.82(2)	
e	7.54(4)	7.528(11)	7.57(3)	
f	7.23(5)	7.22(2)	7.19(5)	
g	7.03(7) (?)	7.05(2)	7.02(5)?	
h	6.80)6)	6.839(10)	6.84(2)	
i	6.60(6)	6.58(2)	6.64(3)	
j	6.35(7)	6.34(2)	6.32(3)	
k	6.13(8) (?)	6.10(2)	6.13(3)	
l	6.03(7)	5.99(2)	6.03(3)	
m	5.83(7)	5.82(2)	5.84(3)	
n	5.71(7)	5.70(2)	5.72(3)	
o	5.30(10)	5.31(2)	5.31(3)	
p	4.20(10)		4.20(4)?	
q	3.95(7)		4.05(4)?	
r			3.67(3)?	
s	3.19(5)		3.17(6)?	
t	3.01(6)		3.03(4)?	
u	2.58(7)			2.68(3)
v	2.11(6)		2.15(3)?	2.06(3)
x			1.75(3)?	
			1.53(3)?	
	1.16(10)		1.10(3)?	1.24(3)
	0.86(8)			0.86(3)
	0.47(6)		0.467(8)	0.45(3)
			0.436(15)	
	0.35(4)		0.330(15)	
	0.29(3)		0.280(15)	

[a]See reference 73
[b]See reference 32
[c]See reference 36

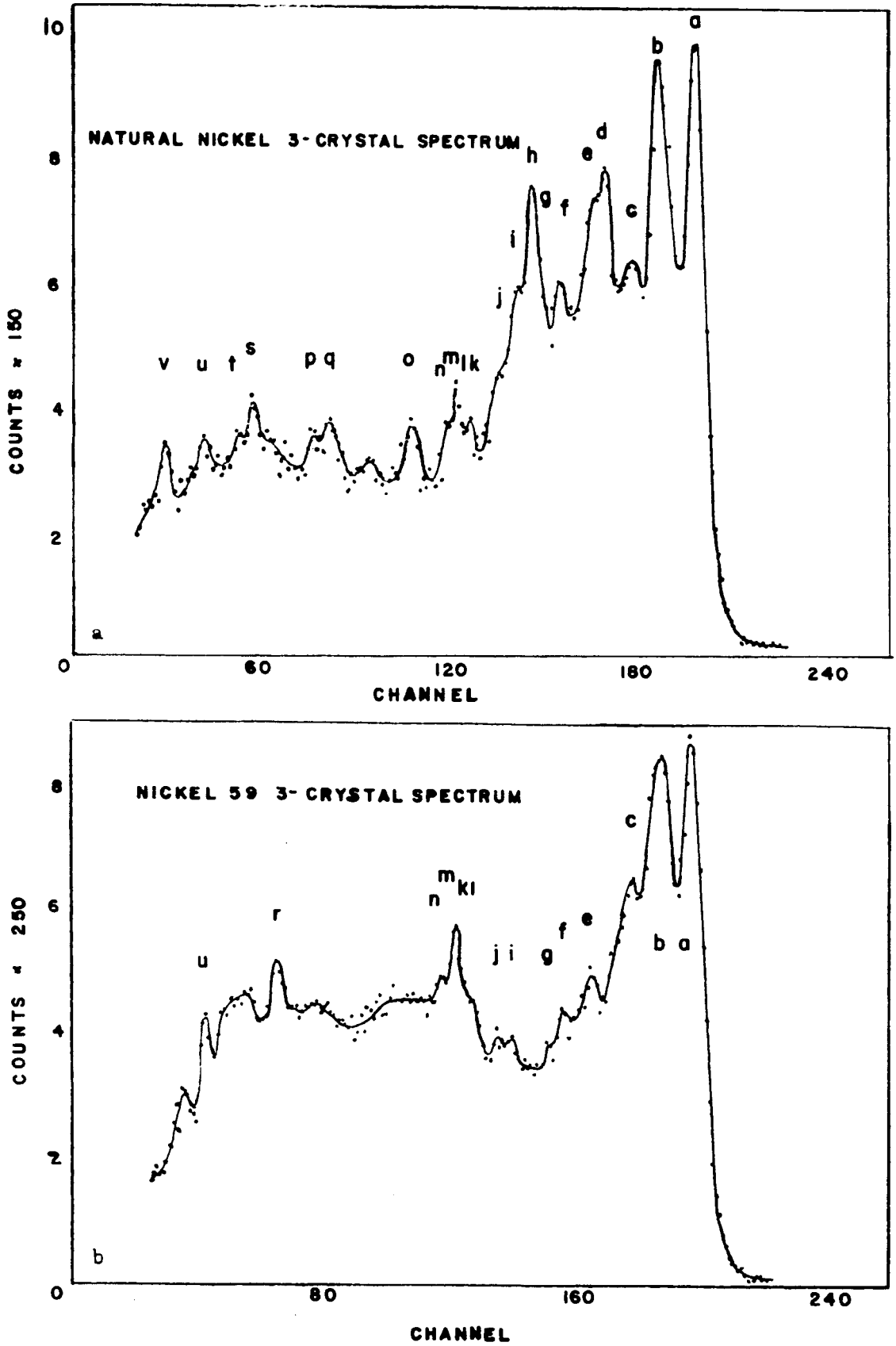

Figure 23. 3-crystal neutron-capture gamma-ray spectra of (a) Natural Nickel and (b) Nickel 59.

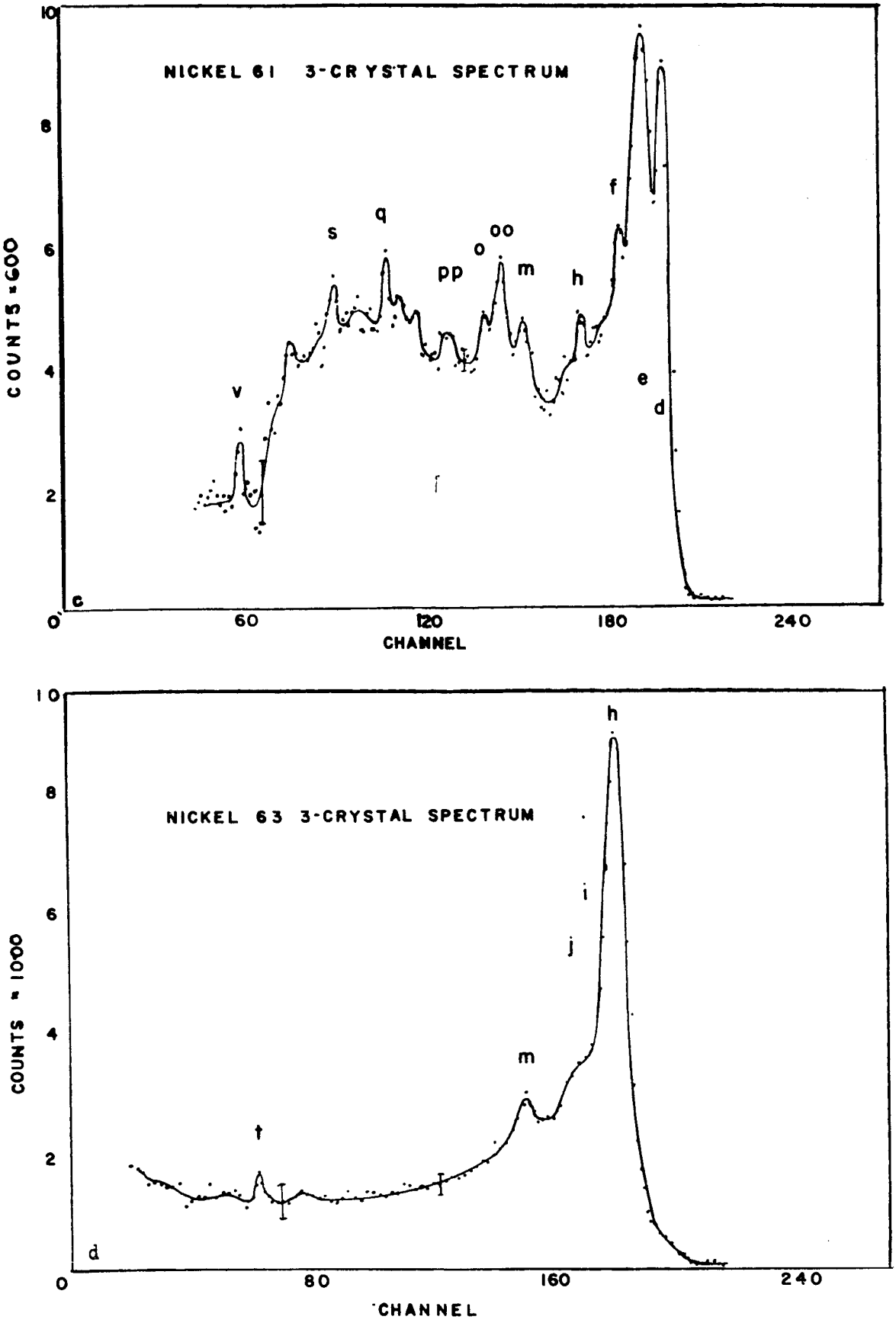

Figure 23. 3-crystal neutron-capture gamma-ray spectra of (c) Nickel 61 and (d) Nickel 63.

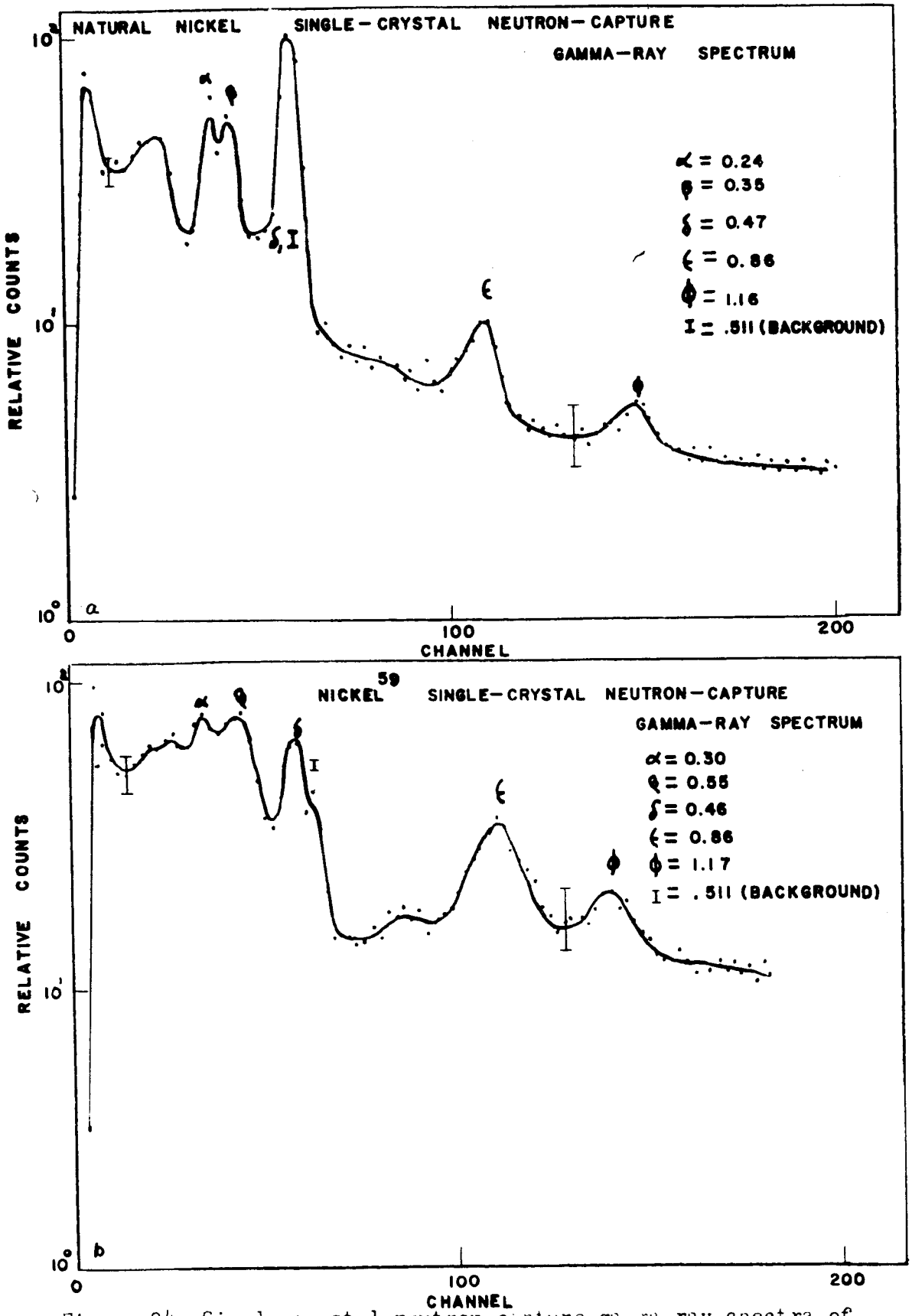

Figure 24. Single-crystal neutron-capture gamma-ray spectra of (a) Natural Nickel and (b) Nickel 59

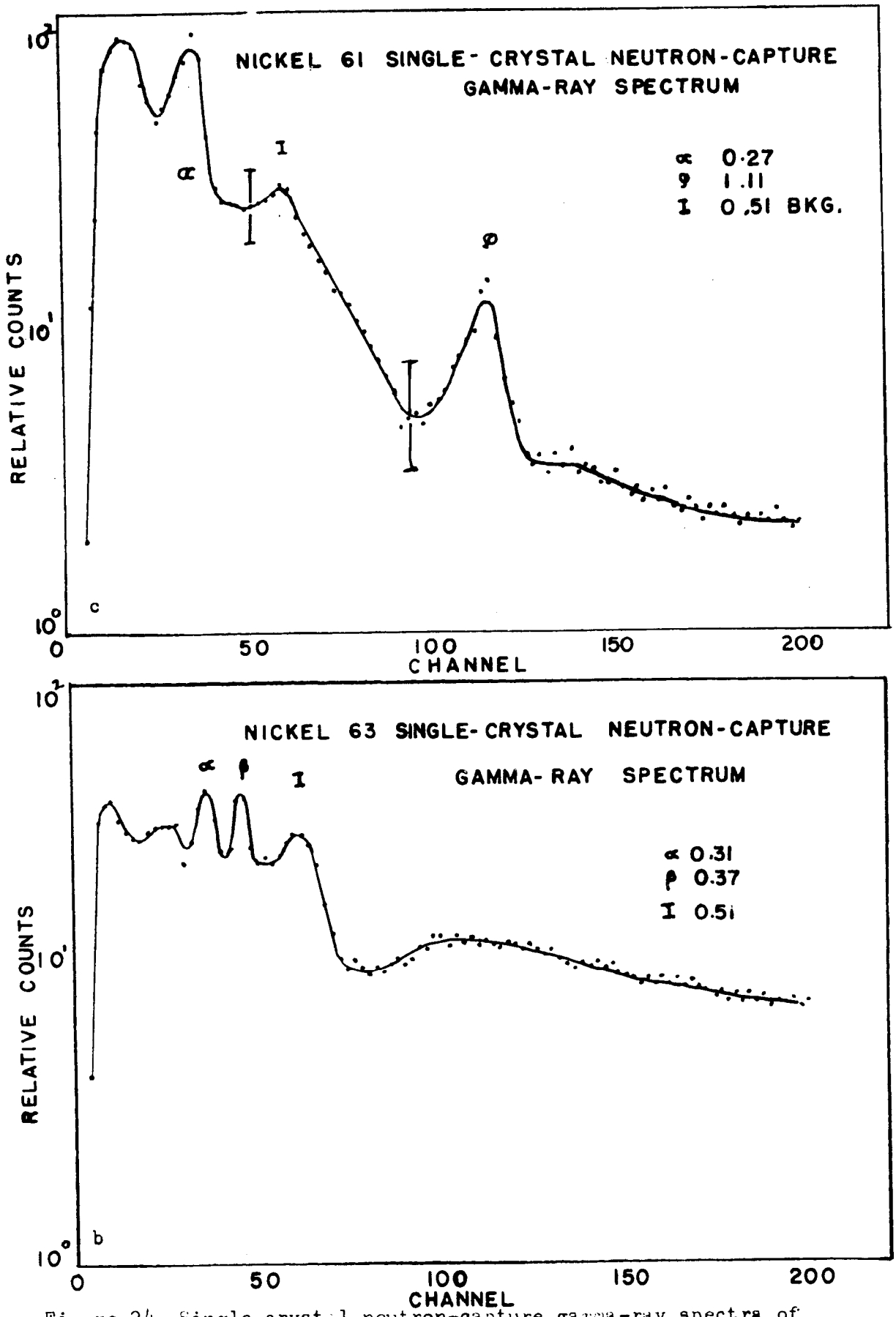

Figure 24. Single-crystal neutron-capture gamma-ray spectra of (c) Nickel 61 and (b) Nickel 63

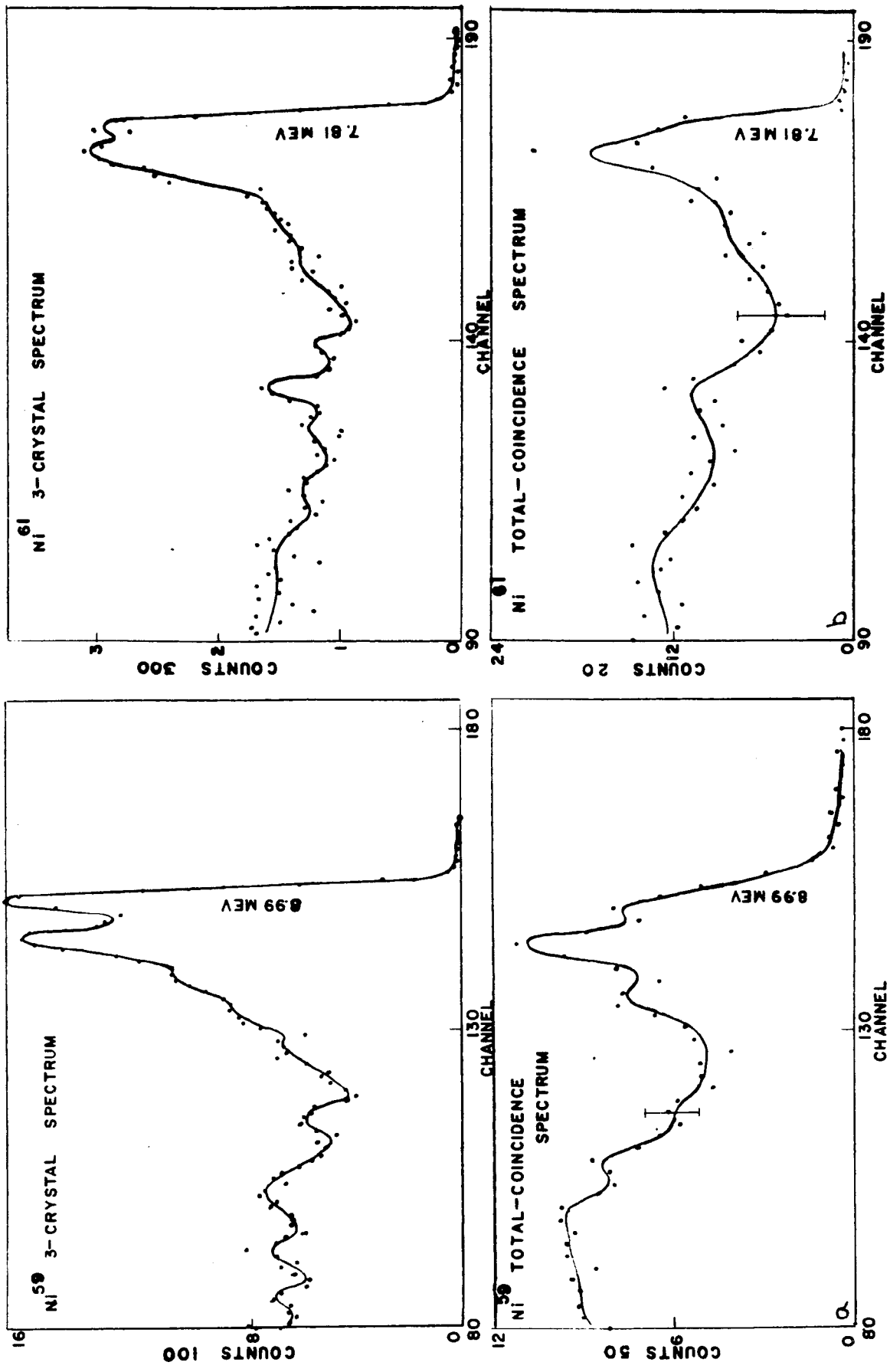

Figure 25. Total coincidence spectra of (a) NICKEL 59 and (b) NICKEL 61.

In interpreting the separated isotope spectra, a gamma ray was assigned to a particular isotope and listed in Table XII if: (a) it had an energy corresponding to a natural nickel gamma-ray energy, and (b) the counting rate in the peak exceeded that in the corresponding valley by at least 3 times the standard deviation. In cases where two isotopes seemed to have the same energy gamma ray, data from $Ni^{58}(d,p)Ni^{59}$ and $Ni^{60}(d,p)Ni^{61}$ were consulted. If a level existed there which was compatible with the energy of the gamma ray, the assignment was made in agreement with the (d,p) data. Many of the gamma rays observed correspond to transitions observed in (d,p) experiments. The gamma rays and corresponding (d,p) proton groups are listed in Table XIII.

Intensities, also given in Table XII, were calculated by assuming cross sections of 4.3, 2.6, and 15 barns for Ni^{58}, Ni^{60} and Ni^{62}, respectively.

TABLE XII

Energies (E_γ) in Mev and intensities (I_γ), in photons per 100 captures in the individual isotope, of the neutron-capture gamma rays from separated nickel isotopes. Uncertainty in the last given digit is indicated in parentheses.

	Natural nickel	$Ni^{58}(n,\gamma)Ni^{59}$		$Ni^{60}(n,\gamma)$	Ni^{61}	$Ni^{62}(n,\gamma)Ni^{63}$	
Key	E	E	I	E	I	E	I
a	8.99(1)	8.99(1)	26(9)				
b	8.53(4)	8.54(4)	19(7)				
c	8.14(4)	8.15(4)	11(6)				
d	7.82(4)			7.81(2)	12(4)		
e	7.54(4)	7.65(6)	9(4)	7.52(3)	13(4)		
f	7.23(5)	7.24(6)	8(4)	7.18(5)	7(5)		

g	7.03(7)?	7.00(7)?					
h	6.80(6)			6.72(10)	7(3)	6.80(2)	62(14)
i	6.60(6)	6.57(8)	7(4)			6.50(12)[a]	
j	6.35(7)	6.30(8)	6(3)			6.35(12)[a]	
k	6.13(8)?	6.08(10)[a]	5(3)				
l	6.03(7)	5.97(10)[a]	5(3)				
m	5.85(7)	5.81(6)	15(7)	5.79(10)	3(2)	5.88(5)	8(4)
n	5.71(7)	5.65(9)	6(3)				
oo[b]				5.55(5)	9(4)		
o	5.30(10)			5.28(8)	8(4)		
pp[b]				4.70(10)	7(4)		
p[c]	4.20(7)						
q	3.95(7)			3.94(10)?			
r[b]		3.70(10)?					
s	3.19(5)			3.20(5)?			
t	3.01(6)					3.01(7)?	
u	2.58(7)	2.65(18)?					
v	2.11(6)			2.25(10)?			
	1.16(10)	1.17(10)		1.11(8)			
	0.86(8)	0.86(3)					
	0.47(6)	0.46(3)					
	0.35(4)	0.35(4)				0.37(3)	
	0.29(3)	0.30(4)		0.27(3)		0.31(3)	

a Unresolved doublet.
b Not observed in natural nickel.
c Not observed in Ni^{58}, Ni^{60}, or Ni^{62}.

The level schemes of the nickel isotopes have been studied by (d,p) reactions[74-78], and radioactive decay of neighboring nuclei[79]. According to these data, the ground-state gamma-ray energies should be 8.99 Mev for Ni^{59} and 7.80 Mev for Ni^{61}. Mass-spectroscopic measurements by Quisenberry et al.[69] indicate that the binding energies should be 8.99 Mev, 7.77 Mev, and 6.82 Mev for Ni^{59}, Ni^{61}, and Ni^{63}, respectively. In the present work, the highest-energy gamma ray found in each isotope should be the ground-state gamma ray. These gamma rays should be quite intense, because the capture state in all three

isotopes has J = $\frac{1}{2}$, as the target nuclei are all even-even, and the ground state spins of Ni^{59} and Ni^{61} are J = 3/2 and that of Ni^{63} is J = 5/2, as stated in the Appendix. Total-coincidence spectra were measured with the Ni^{58} and Ni^{60} samples and in both spectra the highest-energy gamma ray was clearly depressed. From this experiment then, the neutron binding energy for Ni^{59} is 8.99 Mev, for Ni^{61} is 7.81 Mev, and for Ni^{63} is 6.80 Mev.

TABLE XIII

Comparison of capture gamma-ray energies (E_γ) with excitation energies (E_x) from (d,p) reactions in Ni^{58} and Ni^{60}. Assignments are in terms of the product nucleus. Energies are in Mev

Present Results		(d,p) Results		
E_γ	Assignment	E_x	Assignment	Reference
		9.01	Ni^{59}	c,d
8.99	Ni^{59}	8.99	Ni^{59}	b
		8.92	Ni^{59}	a
		8.67	Ni^{59}	d
		8.58	Ni^{59}	b
8.52	Ni^{59}	8.54	Ni^{59}	d
		8.53	Ni^{61}	e
		8.50	Ni^{59}	a
		8.19	Ni^{59}	a
8.14	Ni^{59}	8.13	Ni^{59}	d
7.81	Ni^{61}	7.82	Ni^{61}	d,e
		7.82	Ni^{59}	d
		7.78	Ni^{59},Ni^{61}	a
		7.75	Ni^{61}	d
7.52	Ni^{61}	7.54	Ni^{61}	d
7.24	Ni^{59}	7.23	Ni^{59}	d
7.18	Ni^{61}	7.16	Ni^{61}	d
7.00	Ni^{59}	7.06	Ni^{59}	d
6.72	Ni^{61}	6.72	Ni^{61}	d
6.57	Ni^{59}	6.59	Ni^{59}	d
6.30	Ni^{59}	6.38	Ni^{59}	d
5.97	Ni^{59}	5.97	Ni^{59}	d

5.81	Ni^{59}	5.80	Ni^{59}	d
5.79	Ni^{61}	5.69	Ni^{61}	d
5.28	Ni^{61}	5.21	Ni^{61}	d

[a] see reference 74 , [b] see reference 75, [c] see reference 76
[d] see reference 77, [e] see reference 78

The spectra of the nickel isotopes all had intense high-energy lines and were similar to the spectrum of natural copper; hence anomalous resonance capture as well as direct capture probably occurred. Lane and Lynn[44] calculated that the direct capture cross-section should be approximately 3%, 7%, and 1% of the total capture cross section for Ni^{58}, Ni^{60} and Ni^{62}, respectively. The anomalous resonance contribution was probably comparable to the direct capture one, depending on the effect of the 2p-state in each nuclei. The spectra are in qualitative agreement with the predictions.

E. Tungsten Isotopes

The gamma ray spectrum following thermal-neutron capture in natural tungsten has been investigated by Kinsey et al.[31] and Groshev et al.[59], using external conversion spectrometers. Trumpy[30] investigated the circular polarization of one gamma ray, thought to be from W^{183}, following polarized neutron capture in natural tungsten. Because these experiments required large samples, no separated-isotope studies were done. In the present work, natural tungsten in the form of metallic tungsten powder and W^{182}, W^{184} and W^{186} in the form of isotopically enriched tungsten oxide were irradiated in the neutron beam.

The capture cross-sections, masses, and isotopic constitutions of the samples used are given in Table XIV. The three-crystal spectra, measured over a period of many days, are shown in Figures 26a, 26b, 26c, and 26d. The single crystal spectra, measured for five minutes on each of three operating days, are shown in Figures 27a, 27b, 27c, and 27d. A total-coincidence spectrum was measured with each of the separated-isotope samples. They, along with three-crystal spectra obtained with no side-counter energy discrimination, are shown in Figures 28a, 28b and 28c.

The gamma-ray energies and intensities per 100 neutrons captured of the high energy gamma rays, taken from Figures 26 and 27, are listed in Table XV. No intensities are given for the low energy gamma rays because it was not possible to determine the background contribution to the observed spectrum.

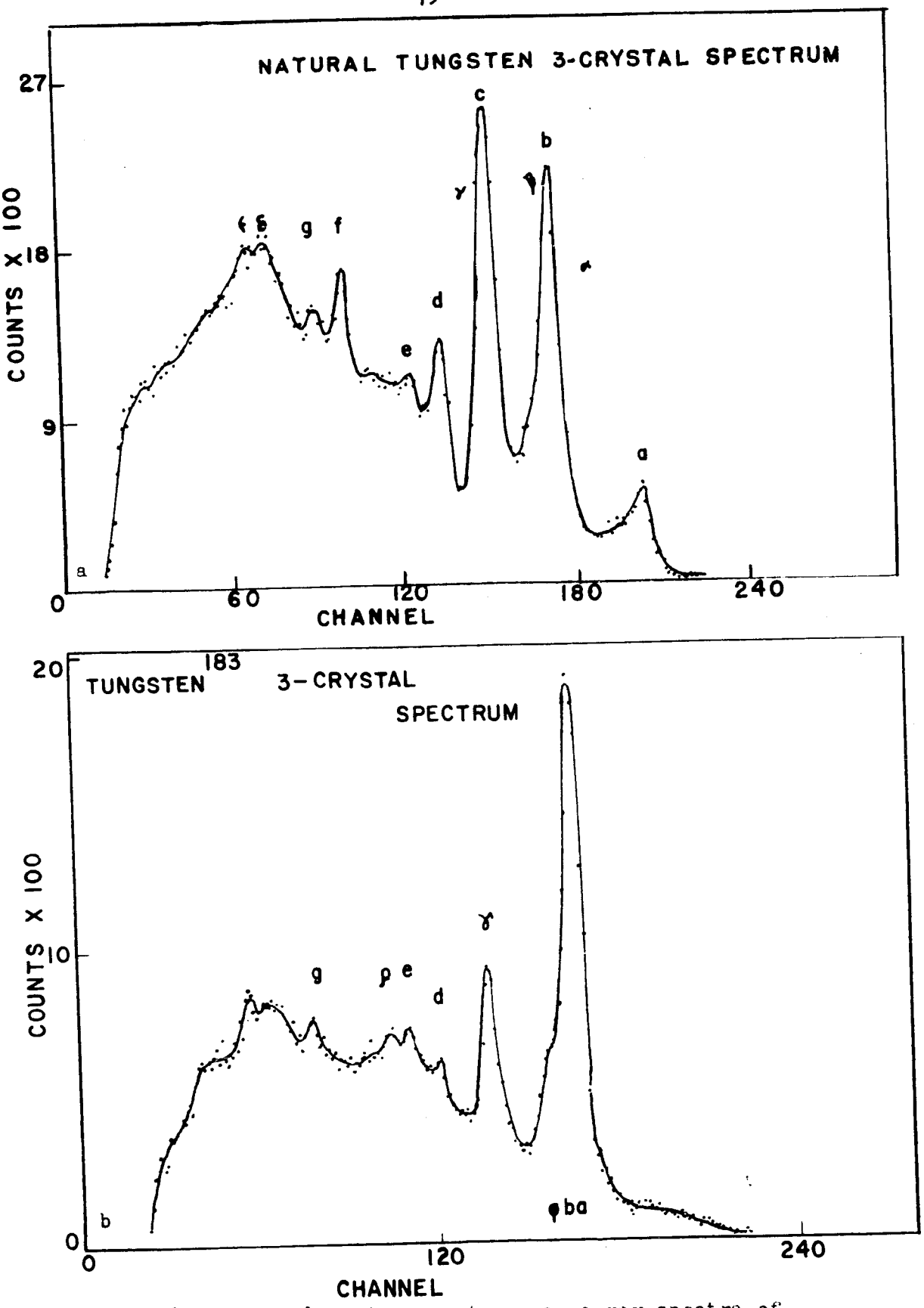

Figure 26. 3-crystal neutron-capture gamma-ray spectra of (a) Natural Tungsten and (b) Tungsten 183.

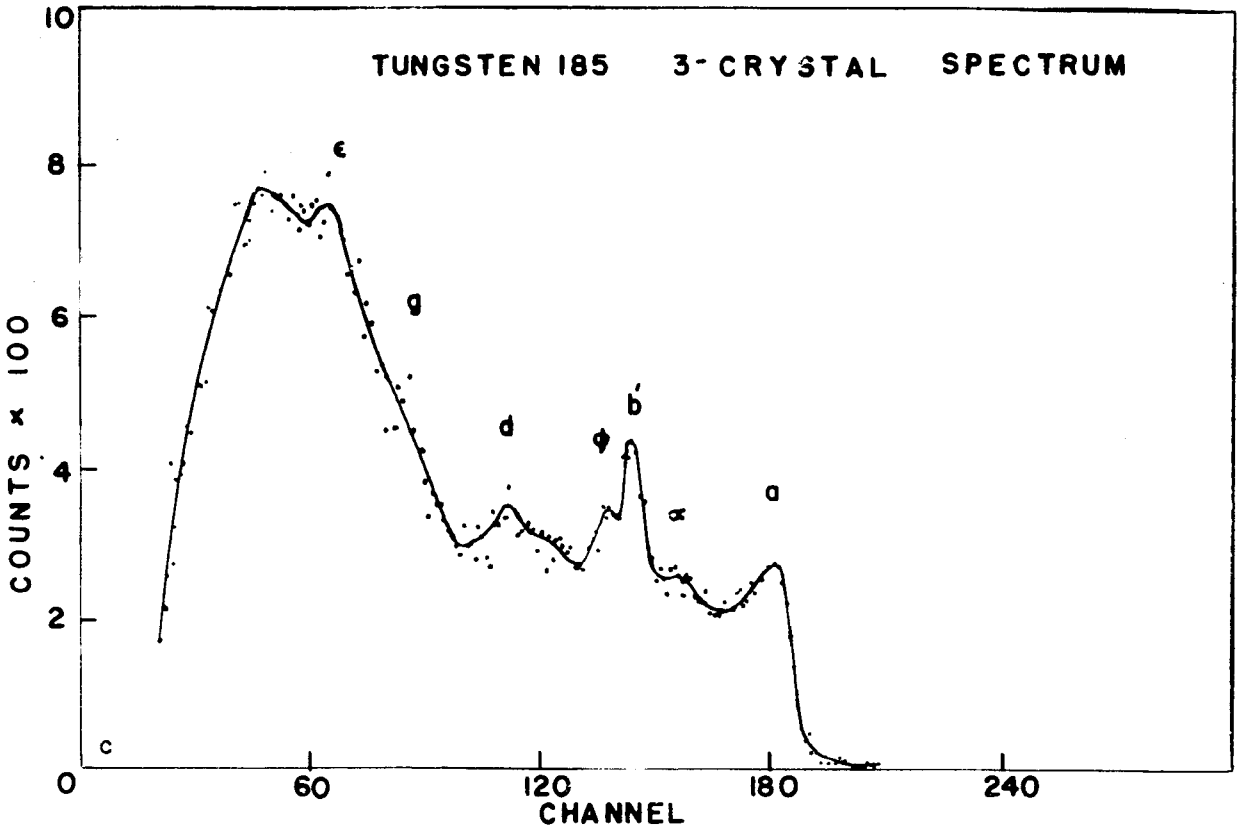

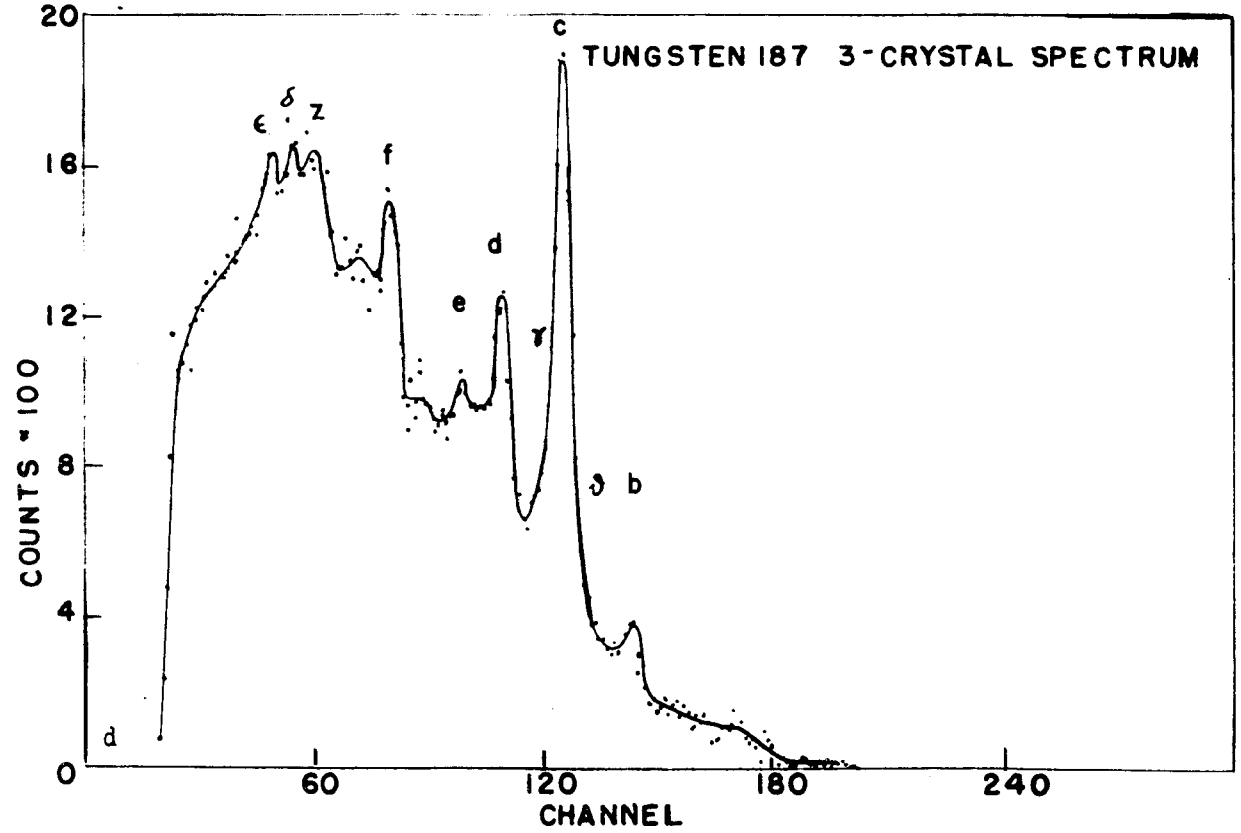

Figure 26. 3-crystal neutron-capture gamma-ray spectra of (c) Tungsten 185 and (d) Tungsten 187.

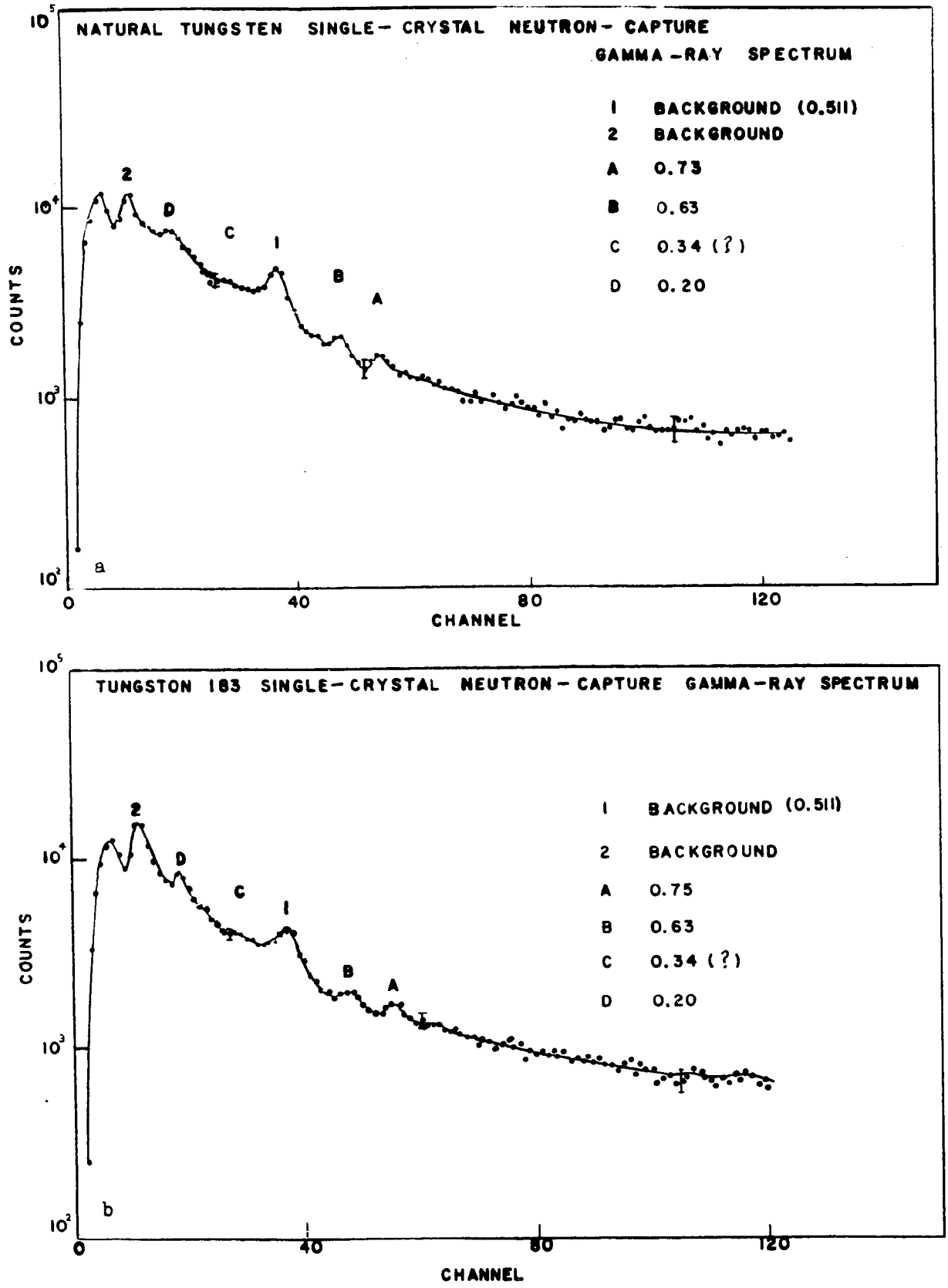

Figure 27. Single-crystal neutron-capture gamma-ray spectra of (a) Natural Tungsten and (b) Tungsten 183.

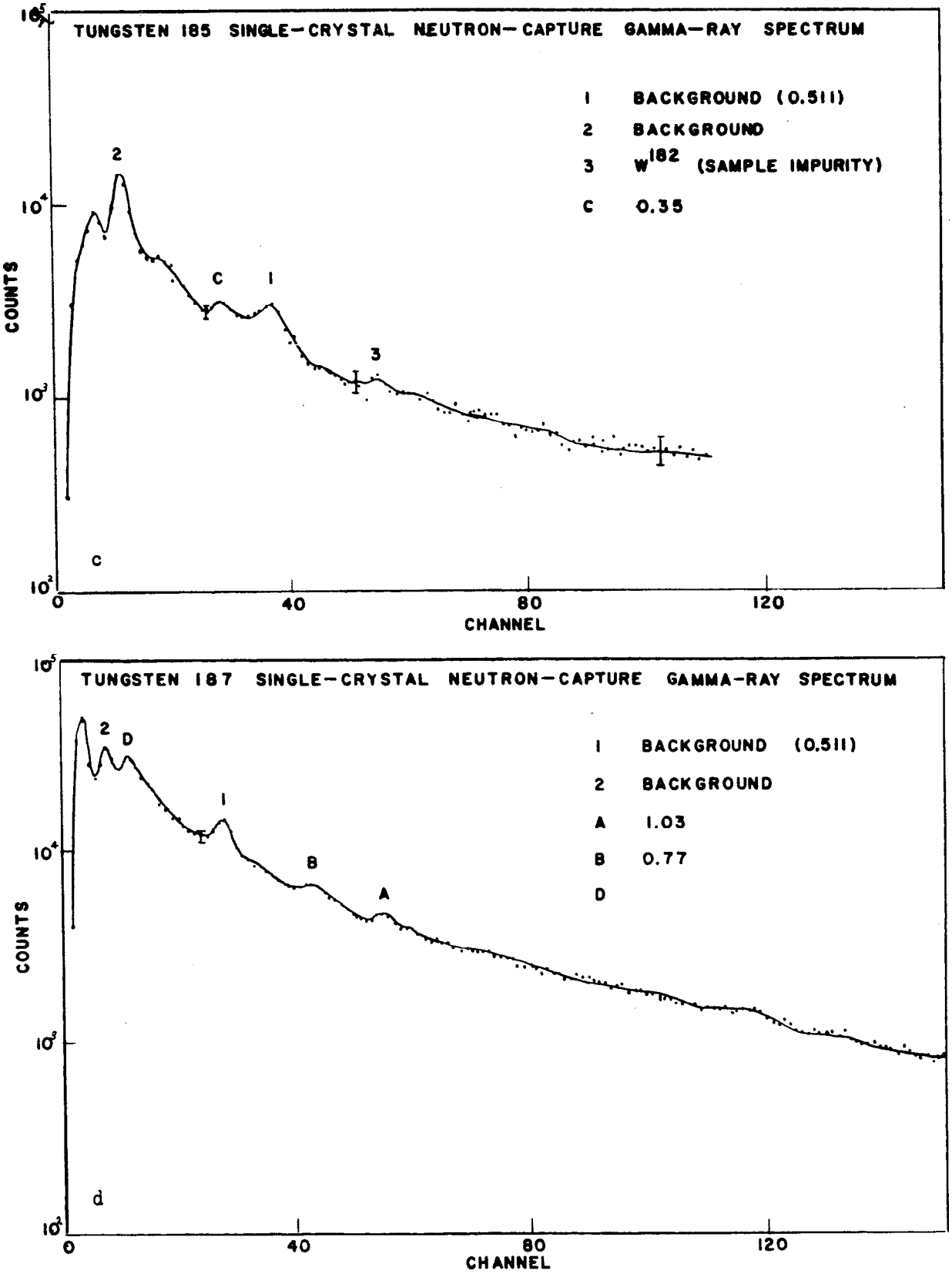

Figure 27. Single-crystal neutron-capture gamma-ray spectra of (c) Tungsten 185 and (d) Tungsten 187.

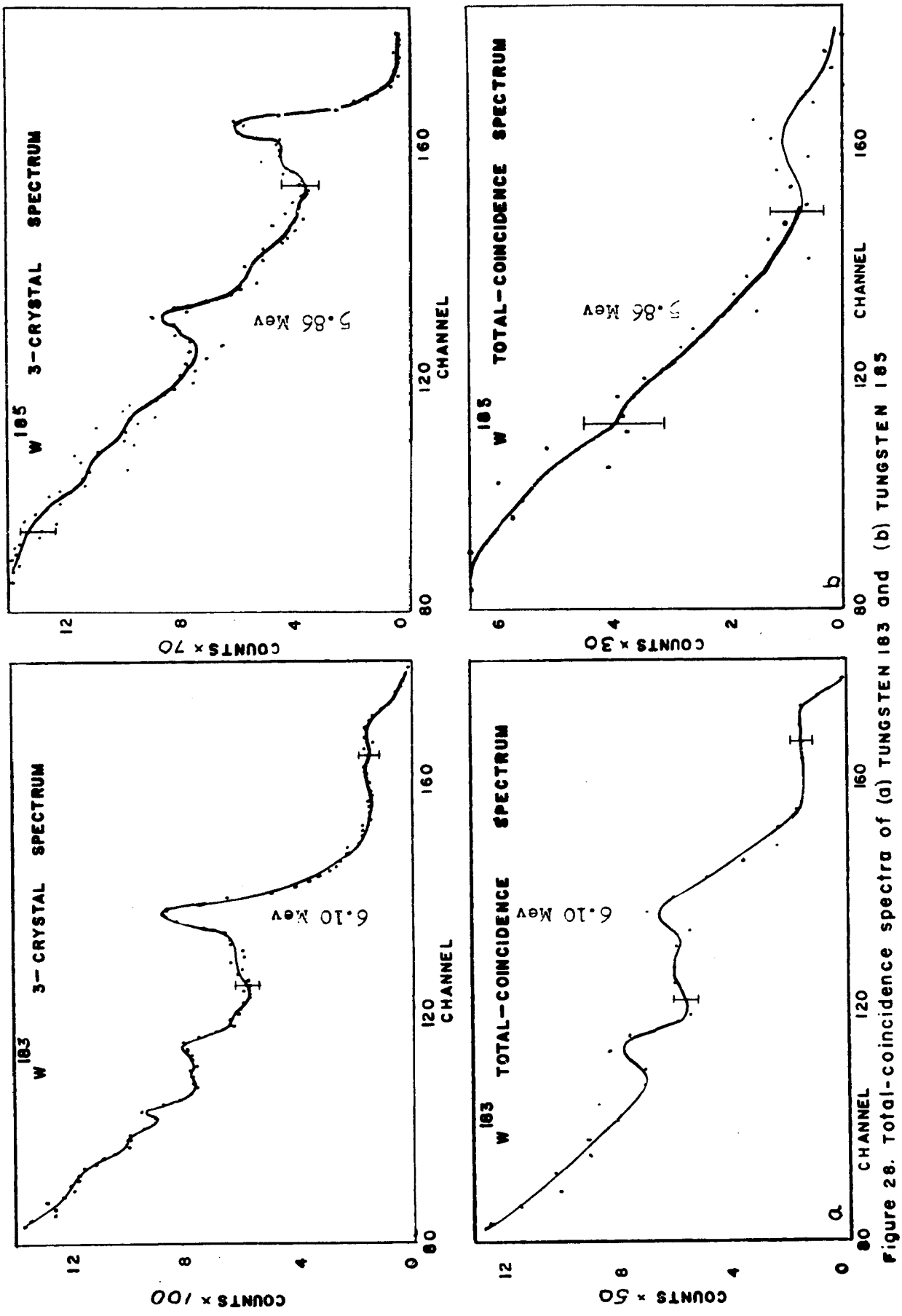

Figure 28. Total-coincidence spectra of (a) TUNGSTEN 183 and (b) TUNGSTEN 185

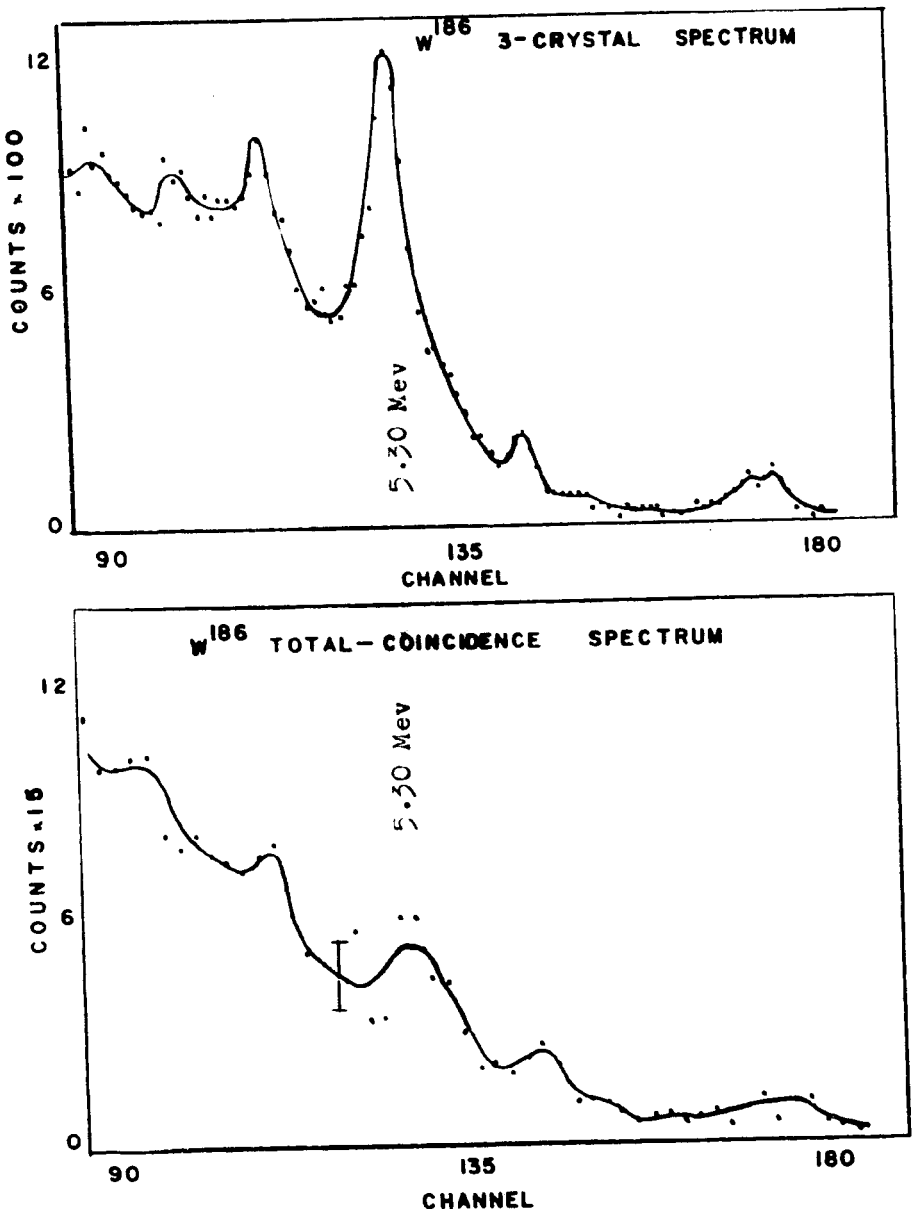

Figure 28c. Total-coincidence spectrum of Tungsten 187.

TABLE XIV

Cross sections, masses and isotopic constitution of the tungsten samples. The chemical impurities in each sample were less than 0.3%.

Sample (Nominal)	σ * (Barns)	Mass (Grams)	Constitution(%) W^{181}	W^{182}	W^{183}	W^{184}	W^{186}
Natural	18	7.8	0.14	26.2	14.3	30.7	28.7
W^{182}	20	5.2	0.03	91.0	4.7	3.4	0.9
W^{184}	2	4.3	0.01	1.1	1.6	95.0	2.3
W^{186}	36	5.4	0.01	0.3	0.3	1.9	97.5

*σ of W^{183} is 11 barns

TABLE XV

Energies in Mev and intensities, in photons per 100 captures in the individual isotope, of the neutron-capture gamma rays from separated tungsten isotopes.

	Present Results[a]							Groshev[b,c]		Kinsey[d]	
	W^{Nat}	W^{183}		W^{185}		W^{187}		W^{Nat}		W^{Nat}	
Key	E	E	I	E	I	E	I	E	I	E	I
a	7.48			7.49				7.43	0.5		
										6.73	0.1
α	6.38	6.35*		6.48*				6.42	0.4	6.40	0.3
								6.19	3.0	6.182	3.8
b	6.16	6.10	6(3)			6.08**	.8(.6)	6.15	2.0		
β	5.98			5.86	2(1)			6.03	0.7	6.02	0.3
		5.72*	1(.8)					5.76	0.3	5.77	0.3
						5.34	3(2)	5.50	0.2		
c	5.26			5.40	1(.6)	5.26	6(4)	5.33	2.5	5.30	2.4
								5.25	3.7	5.25	3.4
γ	5.13	5.16	2(1)					5.17	1.8	5.14	2.3
						5.06	2(1.5)	5.08	0.5	4.94	0.6
								4.70	0.8		
d	4.62	4.56	1(.8)	4.68	2(1)	4.73	5(3)	4.67	1.7	4.67	2.4
e	4.23	4.28	1(.8)			4.31	4(3)	4.25	1.1		

		4.03	2(1.5)				
						3.86	0.6
f	3.51			3.56	5(3)	3.57	2.1
g	3.24	3.19*		3.28	5(3)		
δ	2.76			2.76			
ε	2.58			2.68(?)		2.54	
Z						2.95	
						1.03	
	0.73	0.75				0.77	
	0.63	0.63					
	0.35	0.34		0.34			
	0.20	0.20				0.24	

[a] Roman and Greek letters denote resolved and partially resolved lines, respectively, in natural tungsten.
[b] See reference 59
[c] For lines of energy 4.70 Mev, the intensity is at least as great as the quoted value.
[d] See reference 51
* Not well resolved: ** Due to impurities

Mass spectroscopic measurements by Johnson and Bhanot[80] indicate that the binding energies should be 6.29 and 7.45 Mev for W^{183} and W^{184}, respectively. Martin[64] found the binding energies to be 6.24, 7.45, 5.96, and 5.70 Mev for W^{183}, W^{184}, W^{185} and W^{187}, while Wapstra et al.[65], using all existing data, found 6.19, 7.46, 6.80, and 5.40 Mev to be the binding energies of W^{183}, W^{184}, W^{185} and W^{187}. Dancoff and Kubitschek[15], using geiger counters and aluminum absorbers, found a 6.9 Mev capture gamma ray from natural tungsten and assumed it was the binding energy of W^{187}. In the present work, the total-coincidence spectra were used to determine the binding energies to be 6.10, 7.48, 5.86 and 5.54 Mev for W^{183}, W^{184}, W^{185} and W^{187}. The various binding energies are listed in Table XVI.

TABLE XVI

Neutron binding energies of Tungsten

Isotope	Present Results	Groshev[a] et al.	Kinsey[b] et al.	Martin[c]	Wapstra[d] et al.	Johnson[e] et al.	Dancoff[f] et al.
W^{183}	6.10	6.29		6.24(.50)	6.19(.01)	6.29(.06)	
W^{184}	7.48	7.45	7.42	7.45(.50)	7.46(.14)	7.45(.06)	
W^{185}	5.86	5.60		5.96(.50)	6.8(1.5)		
W^{187}	5.34	5.31	5.31	5.60(.50)	3.4(1.5)		6.9

[a] See reference 59, [b] See reference 31, [c] See reference 64
[d] See reference 65, [e] See reference 80, [f] See reference 15

Although these gamma rays were clearly depressed in the total coincidence spectra, some doubt remains about the binding energies of W^{185} and W^{187}. In W^{184}, the capture state has $J = 1/2^+$ and the ground state has $J = 7/2^-$, so the ground state decay should be relatively weak. Also, the capture cross section of W^{184} is small and the sample impurities (W^{182}, W^{183}, and W^{186}) contributed a line at 6.05 Mev, the line at 6.48 Mev and 50% of the line at 7.49 Mev. The background had a high intensity at 7.5 Mev due to the Pb and Li capture radiation. Consequently, the proportion of the line at 7.49 Mev which had to be from W^{185} was of the order of the statistics. Thus the highest energy gamma ray that was definitely from W^{185} was at 5.86 Mev and, as it was depressed in the total-coincidence spectrum, it must have been the ground state decay. In W^{187}, the capture state to gound state spin change is 0 or 1;

consequently a strong gamma ray should be observed. An intense doublet exists at 5.30 Mev and the highest energy gamma ray of the pair is at 5.34 Mev. This must be the ground state decay.

The binding energy of W^{184} was assumed to be 7.48 Mev as no strong line existed there in any of the separated isotope spectra, while one was observed in the natural tungsten spectrum.

Some lines observed were due to isotopes other than the nominal one. The line at 6.08 Mev in W^{187} was due partially to W^{185} and partially to the tantalum impurity in the sample. The lines at 7.48 and 7.42 Mev in W^{183} and W^{185} have been attributed to W^{184}.

The spectra all have high energy structure which implies that both direct capture and anomalous resonance capture contributed to the capture cross section. If a simple shell model would apply, the spectra could be used to determine the $P_{3/2} - I_{13/2}$ level spacing. However, in the vicinity of A = 170 to A = 185, the nuclei have large deformations, and the level structure is best predicted by the collective model. But a $5P_{3/2}$ state could be accessible in all tungsten nuclei, which would allow appreciable direct capture, and anomalous resonance capture cross sections. At this time there is not enough supplementary information to use the spectra of this experiment to determine quantitatively the relative importance of the two mechanisms.

When more information on deformations and calculated level structures is available, the spectra of iridium and tungsten as well as those of copper and nickel could be used to investigate nuclear capture properties in detail.

APPENDIX

Properties of the Nuclei Studied in this Research

Target Nucleus	Natural Abundance %	σ barns	$T_{1/2}$(product)	J(π), ground state target	product
Br^{79}	50.5	2.9(8.5)	18m (4h*)	3/2	1^+, (5)
Br81	49.5	2.6	35.5h	3/2⁻	5⁻
Cu^{63}	69.1	4.5	12.8h	3/2⁻	1^+
Cu^{65}	30.9	2.1	5.1m	3/2⁻	1^+
Ir^{191}	38.5	960	74d (1.5m)	3/2⁺	5⁻
Ir^{193}	61.5	150	19h	3/2⁺	1⁻
Ni^{58}	67.8	4.2	$8.1C^4$y	0⁺	3/2⁻
Ni^{60}	26.2	2.5		0⁺	3/2⁻
Ni^{62}	3.7	21.0	85y	0⁺	5/2⁻
W^{182}	26.4	19.2		0⁺	7/2⁻
W^{183}	14.4	11.1		1/2⁻	0⁺
W^{184}	30.6	2.0		0⁺	7/2⁻
W^{186}	28.4	34.0	24h	0⁺	1/2⁻

The product nuclei of bromine were odd-odd, while those of copper and iridium were odd-even, and those of nickel and tungsten were even-odd, except W^{184} which is even-even.

BIBLIOGRAPHY

1. D.E. Lea, Nature 133, 24 (1934)

2. E. Amaldi, O. d'Agostino, E. Fermi, B. Pontecorvo, F. Rasetti, and E. Segre, Ricerca Sc. 2, 467 (1934); Proc. Roy. Soc. (London) A149, 522 (1935)

3. R. Fleischmann, Zeit. F. Phys. 97, 242 (1935); Zeit. F. Phys. 97, 265 (1935); Zeit. F. Phys. 103, 113 (1936)

4. F. Rasetti, Zeit. F. Phys. 97, 64 (1935)

5. S. Kikuchi, K. Husimi, and H. Aoki, Proc. Phys.-Math. Soc. Japan 18, 188 (1936)

6. S. Kikuchi, H. Takeda and J. Itoh, Proc. Phys.-Math. Soc. Japan 19, 43 (1937)

7. J.H.E. Griffiths and L. Szilard, Nature 139, 323 (1937)

8. J. Aoki, Proc. Phys.-Math. Soc. Japan 19, 799 (1937)

9. R. Fleischmann, Zeit. F. Phys. 111, 281 (1938)

10. R. Pringle and G. Isford, Phys. Rev. 83, 467 (1951)

11. R. Pringle, H. Taylor, and K. Roulston, Phys. Rev. 87, 1016 (1952)

12. W. Meyerhof, H. Roderick, and L. Mann, Phys. Rev. 83, 203 (1950)

13. W. Reardon, R. Krone, and R. Stump, Phys. Rev. 91, 334 (1953)

14. C.O. Muehlhouse, ANL Report #4437, (1950)

15. H.E. Rubitschek and S.M. Dancoff, Phys. Rev. 76, 531 (1949)

16. C.K. Moak and J.W.T. Dabbs, Phys. Rev. 75, 1770 (1949)

17. B. Hammermesh, Phys. Rev. 76, 182 (1949)

18. C.Millar, A. Cameron, and M. Glicksman, Can. J. Res. A28, 475 (1950)

19. R. Wilson, Phys. Rev. 80, 90 (1950)

20. B. Hammermesh and V. Hummel, Phys. Rev. 83, 663 (1951); Phys. Rev. 88, 916 (1952)

21. M. Reier and M.H. Shamos, Phys. Rev. 100, 1302 (1955)

22. I.V. Estulin, L.F. Kalinkin and A. S. Melioranskii, Nuclear Physics, 4, 91 (1957); Soviet Physics J.E.T.P. 5, 801 (1957); Soviet Physics J.E.T.P. 31, 886 (1956)

23. E.T. Patronis, Jr. and R. Marshak, Phys. Rev. 115, 1287 (1959)

24. D. Rose, R. Ostrander, and B. Hammermesh Review of Scientific Instr. 28, 231 (1957)

25. R.T. Carpenter, L.M. Bollinger, and T.J. Kennett, Bull. Am. Phys. Soc. II, 2, 165 (1958)

26. R.K. Smither, Phys. Rev. 124, 183 (1961)

27. B. Hammermesh and A.L. Hecksiedler, Phys. Rev. 96, 109 (1954)

28. R.E. Segel, Bull. Am. Phys. Soc. II, 2, 230 (1957); Phys. Rev. 111, 1620 (1958); Bull. Am. Phys. Soc. II, 3, 64 (1958)

29. P.A. Treado and P.R. Chagnon, Phys. Rev. 121, 1734 (1961)

30. G. Trumpy, Nuclear Physics 2, 664 (1957)

31. B.B. Kinsey and G.A. Bartholomew, Can. J. Phys. 31, 1051 (1953); Can. J. Phys. 31, 1025 (1953); in Beta and Gamma Ray Spectroscopy, ed. by K. Siegbahn, Amsterdam: North-Holland Publishing Co., (1955)

32. B.P. Adyasevich, L.V. Groshev, A.E. Demidov, and V.N. Lutsenko, Atomnaya Energia 2, 28 (1957); Atomnaya Energiya 2, 40 (1956,; A.E. Demidov, V.N. Lutsenko, and V.I. Pelekov, Atomnaya Energia 3, 187 (1957); Atomnaya Energia 4, 5 (1958)

33. W. Thornton, E.der Mateosian, R.T. Motz and M. Goldhaber, Phys. Rev. 86, 604 (1952); R.T. Motz, Phys. Rev. 80, 555 (1953); Phys. Rev. 92, 525 (1954)

34. J.W. Knowles, Chalk River Report GP I-42, (1957)

35. G. Manning and G.A. Bartholomew, Phys. Rev. 115, 401 (1959); G. Manning, G.A. Bartholomew, J.W. Knowles, and P.J. Campion, Phys. Rev. 114, 1065 (1959)

36. I.M. Braid, Phys. Rev. 102, 1109 (1956)

37. J.E. Draper and J.K. Bockelman, Bull. Am. Phys. Soc. Ser.II, 3, 177 (1956)

38. S.A.E. Johansson, Phil Mag. 43, 249 (1952)

39. R. Hofstadter and J.A. McIntyre, Phys. Rev. 79, 389 (1950)

40. L.I. Schiff, Quantum Mechanics, New York, 1955

41. E. Fermi, Nuclear Physics, Chicago, 1949

42. N. Bohr, Nature 137, 344 (1936)

43. N. Bohr and P. Wheeler, Phys. Rev. 56 426 (1939)

44. A.M. Lane, Nuclear Physics 11, 625 (1959); A.M. Lane and J.E. Lynn, Nuclear Physics 11, 646 (1959); Nuclear Physics 17, 563 (1960); Nuclear Physics 17, 586 (1960)

45. G. Breit and E. Wigner, Phys. Rev 49, 519 (1936)

46. A.V. Shutko and D.F. Zaretskii, Soviet Physics J.E.T.P. 2, 769 (1956)

47. V.M. Strutinskii, L.V. Groshev, V.N. Lutsenko, A.M. Demidov and V.I. Peledov, Nuclear Physics 1, 281 (1958); V.M. Strutinskii, L.V. Groshev and M.K. Akimova, Soviet Physics J.E.T.P. 11 430 (1960)

48. D. terHaar, Elements of Statistical Mechanics, New York (1954)

49. C. van Lier and G.E. Uhlenbeck, Physica 4, 531 (1937)

50. J.M. Blatt and V.F. Weiskopf, Theoretical Nuclear Physics, New York (1952)

51. A.M. Lane, Atomic Energy Research Establishment Report AERE T/R, 1289 (1954)

52. G.A. Bartholomew, in Nuclear Spectroscopy, ed. by F. Ajzenberg-Selove, New York (19[illegible])

53. A.M. Lane and D.H. Wilkinson, Phys. Rev. 97 1199 (1957)

54. [illegible] Boekelman, Nuclear Physics 13, 205 (19[illegible])

55. P.R. Chagnon, Univ. of [illegible] Res. Inst. Report 2865-1-P, September, 1959 (unpublished)

56. P.R. Chagnon, Rev. Sci. Inst. 32, 68 (1961)

57. H. Jung, Ph. Panussi and J. Janecke, Nuclear Instruments and Methods, 9, 121 (1960)

58. W.R. Kane, private communication; J.E. Schwager, private communication

59. L.V. Grosnev, B.N. Lutsenko, A.M. Demidov, and V.I. Pelekov, Atlas of Gamma-Ray Spectra from Radiative Capture of Thermal Neutrons, Pergamon Press, New York (1958)

60. Nuclear Data Sheets, National Research Council, Washington, D.C. (1959)

61. D.J. Hughes and J.A. Harvey, Neutron Cross Sections, New York (1955)

62. R. Evans, The Atomic Nucleus, New York (1955)

63. P.J. Campion and G.A. Bartholomew, Can. J. Phys. 35, 1361 (1957)

64. C.H. Martin, Nuclear Tables, Paris (1954)

65. L.A. Koenig, J.H.E. MaHauch, and A.G. Wapstra, USAEC 1960 Nuclear Data Tables, Part 2 U.S. Government, Washington, D.C.

66. G.A. Bartholomew and B.B. Kinsey, Phys. Rev. 89, 386 (1953)

67. V.V. Skylarevskii, E.P. Stepanov, and B.A. Obenyakov, Soviet Journal of Atomic Energy 4, 19 (1958)

68. R.P. deFigueiredo, M. Mazeri, and W.W. Buechner, BAPS 3, 38 (1958)

69. K.S. Quisenberry, T.T. Scolman, and A.O. Nier, Phys. Rev 104, 461 (1957)

70. H. Knoepfel, P. Stoll, and P. Scherrer, Zeit. f Phys. 156, 293 (1960)

71. N. Fiebiger, private communication

72. R. Demirkhanov, V. Gutkin, and N. Dorokhov, Soviet Physics J.E.T.P. 37, 1217 (1959)

73. B.B. Kinsey and G.A. Bartholomew, Phys. Rev. 89, 375 (1953)

74. W.W. Pratt, Phys. Rev. 94, 1086 (1954); 95, 1517 (1954)

75. C.E. McFarland, M.M. Bretscher, and F.B. Shull, Phys. Rev. 89, 892 (1953)

76. J.M. Harvey, Phys. Rev. 81, 353 (1951)

77. J.H. Paris and W. W. Buechner, Bull. Am. Phys. Soc 3, 38 (1958)

78. H.N. Hoesterey, Phys. Rev. 87, 216 (1952)

79. G.L. Owen, J.S. Cook, and P. H. Owen, Phys. Rev. 78, 686 (1950)

80. M.H. Johnson and V.B. Bhanof, Phys. Rev. 107, 1669 (1957)